



HAL
open science

Times are changing: A new chronology for Holocene volcanic events and hydro-sedimentary history recorded in the Sarliève marsh (central France)

Alfredo Mayoral Pascual, Gérard Vernet, Olivier Voltaire, Jean-François Berger, Yannick Miras, Emmanuelle Defive

► **To cite this version:**

Alfredo Mayoral Pascual, Gérard Vernet, Olivier Voltaire, Jean-François Berger, Yannick Miras, et al.. Times are changing: A new chronology for Holocene volcanic events and hydro-sedimentary history recorded in the Sarliève marsh (central France). *Quaternary Science Reviews*, 2021, 272, pp.107237. 10.1016/j.quascirev.2021.107237 . hal-03385683

HAL Id: hal-03385683

<https://hal.science/hal-03385683v1>

Submitted on 19 Oct 2021

HAL is a multi-disciplinary open access archive for the deposit and dissemination of scientific research documents, whether they are published or not. The documents may come from teaching and research institutions in France or abroad, or from public or private research centers.

L'archive ouverte pluridisciplinaire **HAL**, est destinée au dépôt et à la diffusion de documents scientifiques de niveau recherche, publiés ou non, émanant des établissements d'enseignement et de recherche français ou étrangers, des laboratoires publics ou privés.

1 Times are changing: a new chronology for Holocene volcanic events and
2 hydro-sedimentary history recorded in the Sarliève marsh (central France)

3
4
5 MAYORAL, Alfredo^{a,b*}; VERNET, Gérard^c; VOLDOIRE, Olivier^a; BERGER, Jean-François^d; MIRAS,
6 Yannick^e; DEFIVE, Emmanuelle^a

7
8
9 (a) CNRS, GEOLAB, Université Clermont Auvergne, Clermont-Ferrand, France.

10 (b) Catalan Institute of Classical Archaeology, Tarragona, Spain

11 (c) Université Clermont Auvergne, CNRS, INRAP, LMV, Clermont-Ferrand, France

12 (d) CNRS, UMR 5600, EVS-IRG & Université Lyon 2, Lyon, France

13 (e) CNRS, UMR7194, Histoire Naturelle de l'Homme Préhistorique, Muséum National d'Histoire
14 Naturelle, Institut de Paléontologie Humaine, Paris, France

15 *Corresponding author. amayoral@icac.cat; alfredo.mayoral@uca.fr

16 **Abstract:** This paper presents the first well-dated palaeoenvironmental study from the Sarliève
17 marsh, a unique sedimentary record in the Limagne plain of central France, where all previous
18 studies suffered from unreliable chronologies. We developed an accurate radiocarbon-based age-
19 depth model and performed high-resolution multi-proxy sedimentological and geochemical analysis
20 on a new sediment core from the heart of the sedimentary basin, improving the chronology and
21 Holocene palaeoenvironmental interpretations. We found six potential (crypto)tephra fallouts (c.
22 9750, 8500, 7500, 7400, 6300, and 5800 cal yr BP) that enrich the Holocene tephrostratigraphy in
23 Limagne, five of which were not previously documented in the sediments of the marsh. We also
24 detected, for the first time, an array of volcanic phenomena such as degassing episodes (c. 6950 and
25 6050 cal yr BP), ash leaching phases (10250–9750, 8500–7400, and 5800–5100 cal yr BP), and

26 earthquakes (c. 6800, 6600, 6050, 6100, and 1600 cal yr BP), suggesting a hitherto unsuspected
27 period of high volcanic activity in the area between 7500 and 5800 cal yr BP. This increased activity
28 appears to have caused a massive forcing of hydrosedimentary dynamics in the catchment in the
29 Middle Holocene, by supplying significant volumes of fine volcanic ash to the palustrine basin, and
30 thereby questioning the current Holocene morpho-sedimentary narrative for Limagne. The basin
31 became a permanent freshwater lake after the Mid-Holocene climatic shift, and detrital influxes
32 likely due to anthropogenic soil erosion appeared c. 5500 cal yr BP and grew steadily after 5000 cal yr
33 BP, with a marked lull between 3600 and 3000 cal yr BP, perhaps because of a phase of settlement
34 abandonments during the middle and early-late Bronze age. A series of lacustrine low-stands (c.
35 4750–4600, 3750–3600, 3350–3200 and 2950–2800 cal yr BP) that correlate strongly with western
36 alpine lake records do not seem to have caused significant changes in the anthropogenic impact on
37 soils modifying the sedimentary supply. Our results suggest that this lake could have been artificially
38 drained c. 2550 cal yr BP, several centuries earlier than previously estimated, allowing us to
39 hypothesize that Early Iron age societies already had substantial capacity to modify the hydraulic
40 environment. Hydromorphic conditions developed thereafter, including complex short-lived marshy
41 phases in late Roman times.

42
43 **Keywords:** Palaeoenvironment, Age-depth modelling, Cryptotephra, Volcanic activity, Hydro-
44 sedimentary processes, Sedimentology, Geochemistry, Socio-environmental interaction, Holocene,
45 Massif Central

46

47

48

49

50

51

52 1. INTRODUCTION

53

54 Over recent decades, studies concerning Holocene palaeoenvironments and socio-environmental
55 interactions have progressed substantially (e.g. Wang et al., 2013; Kaufman et al., 2020). Increasingly
56 robust approaches are often based on nuanced interpretations of case-by-case studies to correctly
57 discuss causality in socio-environmental trajectories (e.g. Lespez et al., 2016). The common spine of
58 these approaches is accurate dating, because precise, reliable, and comparable chronologies are
59 crucial for any interpretation (Blaauw, 2012; Armit et al., 2014). Unfortunately, precise chronological
60 data are still lacking for large areas of Europe, preventing a fine integration between
61 palaeoenvironmental and archaeological datasets.

62 This is typically the case in the intra-mountainous carbonated plain of Limagne in central France,
63 where sedimentary archives adequate for palaeoenvironmental studies are very rare. One of the few
64 exceptions is the Sarliève marsh, where the first studies started in the 1960's (Gachon, 1963). This
65 wetland is a depression located 5 km south of Clermont-Ferrand at the feet of the Chaîne des Puys, a
66 volcanic range that produced several well-known eruptions, tephra fallouts, and lava flows during the
67 Lateglacial and Mid-Holocene (Boivin et al., 2017) (Fig. 1A–B). The basin is nowadays a drained plain
68 with a NW–SE elongated shape and an outlet at its northern border (Fig. 1C). The lithology of the
69 catchment is relatively diverse (Fig. 1D): Miocene basalts, breccias, and tuffs overly the Oligocene
70 carbonated sedimentary rocks of the Limagne formation (BRGM, 1973; Bouiller, 1979). Differential
71 erosion has carved prominent buttes and plateaus topped by volcanic rocks, which dominate the
72 lowlands. The surficial formations include colluvium of variable thickness, nature, and lithology (see
73 Fig. 1D). The lowlands include Pleistocene alluvium from the river Allier (Fig. 1B) and alluvio-colluvial
74 infillings affected by hydromorphy, the so-called “Limagne complex”, in the drained Sarliève
75 depression. The climate is oceanic to semi-continental (Köppen Cfb), with cold and relatively dry
76 winters and hot and stormy summers (Joly et al., 2010). From an archaeological perspective, the

77 sector is relatively well known, and multi-period remains and settlements (Neolithic to late Roman)
78 have been documented around the Sarliève basin, especially at the summit of the Gergovie plateau
79 (Trément et al., 2007).

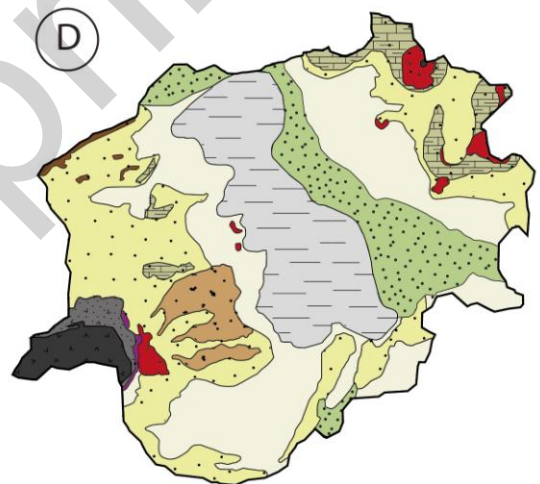
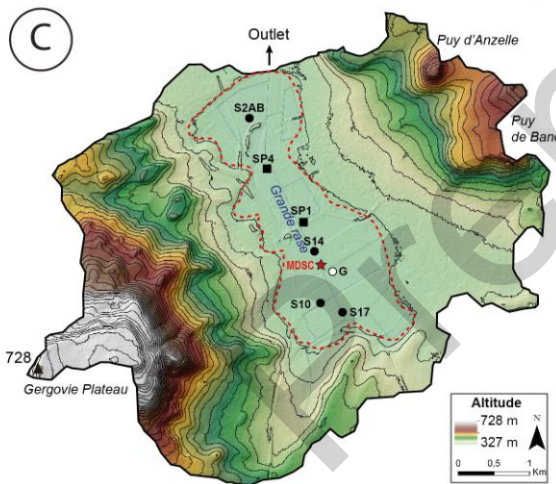
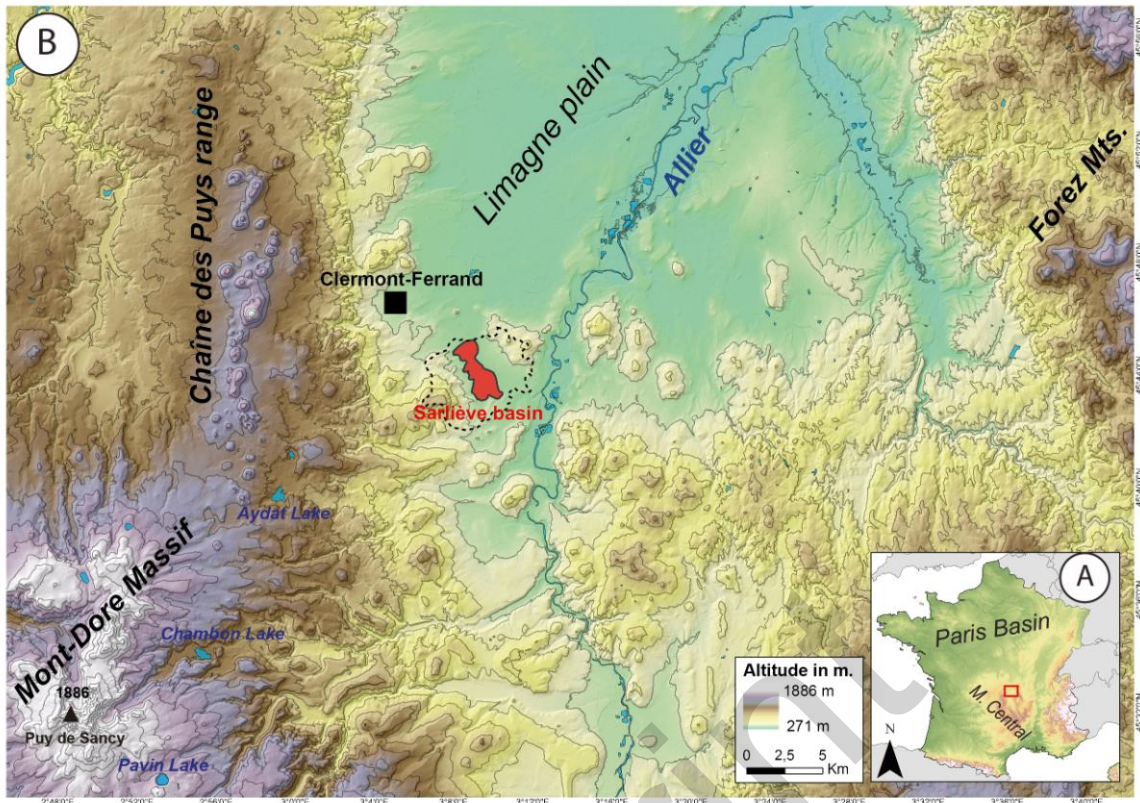
80 The Sarliève marsh was the object of several geological and palaeoenvironmental studies in the
81 2000s. The morphology of the basin and the geometry of its sedimentary infilling are well-known: it is
82 divided into northern and southern sub-basins, which were separated by a threshold during the first
83 half of the Holocene and then connected later, and contain 5 to 6 m of Lateglacial to Holocene fine
84 sedimentary infilling, including several lacustrine phases (Fourmont, 2006; Hirschberger et al., 2006).

85 The palaeohydrological, geomorphological, and sedimentological evolution from the Lateglacial have
86 also been largely documented: four major phases controlled by a combination of climatic (earlier
87 phases) and anthropogenic (later phases) factors have been detected, before the modern drainage of
88 the depression in recent centuries. An endorheic saline lake during the Early Holocene was followed
89 by detrital and laminated facies during the Middle Holocene, indicating highly variable hydro-
90 sedimentary conditions that evolved to a permanent carbonated lake during the Middle to Late
91 Holocene. Finally, the lake was drained in the late Protohistory, although later marshy phases are
92 known (Bréhéret et al., 2003; Vernet, 2005; Fourmont, 2006; Bréhéret et al., 2008; Fourmont et al.
93 2009). The sedimentary budget of the catchment since the Lateglacial has also been addressed, with
94 an acceleration from approximately 5300 cal yr BP being interpreted as anthropogenic (Macaire et
95 al., 2010). Finally, in its peripheral areas, the basin also includes at least two volcanic fallouts,
96 identified as the tephra CF1 (c. 13,000 cal yr BP; Vernet et al., 2011; Vernet, 2013, 2019) and the
97 “Tephra de Sarliève” (uncertain age, around 5000 cal yr BP). Both fallouts were likely to have
98 dissolved in central areas of the basin under aquatic conditions (Miallier et al., 2004; Vernet, 2005;
99 Fourmont et al., 2006). Palaeoenvironmental studies have also been performed on several cores
100 from deeper areas of the marsh or deep test pits (Fourmont, 2006; Prat, 2006; Trément et al., 2007;
101 Macaire et al., 2010), allowing a reconstruction of the vegetation and landscape, hydrological
102 conditions, and human activities since the beginning of the Neolithic. All of the abovementioned

103 studies were integrated into a socio-environmental model for the sector (Trément et al., 2007;
104 Trément, 2011) that was used to discuss the roles of Holocene hydro-climatic variability and human
105 activities on landscape evolution during the Holocene, identifying thresholds in the IInd century BC
106 and Roman periods.

107 Unfortunately, the keystone for the integration of these rich multi-proxy studies in the Sarliève
108 marsh (i.e., the radiocarbon chronology of the sedimentary sequence) was highly unsatisfactory
109 because of uncontrolled ageing, and even after several amendments (Hatté et al., 2013), the age-
110 depth model remained controversial due to its inconsistency with the palynological data and regional
111 vegetation history (see Miras, 2016). This situation is especially critical between the Late Neolithic
112 and Antiquity, because different datasets cannot be correlated, preventing any fine discussion on
113 human-environment interactions during late Protohistory, which is considered a crucial period for
114 the consolidation of anthropogenic impacts on natural systems (Berger et al., 2018; Mayoral, 2018).
115 This situation is especially problematic because it affects a unique lacustrine sequence in the Limagne
116 plain, which represents its only palynological record.

117 The main aim of this work was to construct an accurate and reliable radiocarbon chronology for the
118 sedimentary infilling of the Sarliève marsh, and to use it to carry high-resolution analysis that will
119 allow completion and refinement of the palaeoenvironmental interpretation of this reference
120 sequence. To achieve this task, new cores drilled into the heart of the marsh were radiocarbon-dated
121 using carefully selected materials and were subjected to multi-proxy sedimentological and
122 geochemical analyses. These new developments are integrated, interpreted and discussed together
123 within an accurate chronological framework provided by a Bayesian age-depth model.



Selected sedimentary sequences

- ★ MDSC core (this study, Dec. 2018)
- S cores (A. Fourmont, 2000-2005)
- SP survey pits (INRAP, 1999-2005)
- G core (Lo. Gachon, 1963; repeated by C. Ballut, 1997)
- Extent of the marshy area

Bedrock

- Basalts (Miocene)
- Gergovie formation: marls, clays, sands, limestones, sandstones (Miocene)
- Peperitic breccia and tuffs (Olig.-Mioc.)
- Limagne formation: marls, clays, limestones, sands (Oligocene)

Surficial formations

- Limagne hydrom. complex (alluvio-colluvial)
- Pleistocene alluvium (Fw and Fv)
- Volcanic colluvium
- Landslides on volcanic materials (complex)
- Volcano-sedimentary dejection materials
- Fine carbonated colluvium of lower slopes
- Colluvium s.l. from marls, clays and limestones

124

125

126

127

Figure 1. A) Location of the study area in central France. B) Location of the Sarliève basin in the southern Limagne plain. C) Topography of the Sarliève catchment and location of main sedimentary sequences studied since 1963. D) Geology of the Sarliève catchment (after Fourmont et al., 2009 and Macaire et al., 2010)

128 2. MATERIALS AND METHODS

129

130 *2.1. Coring and litho-stratigraphic description*

131

132 The coring was implemented in the depocenter of the southern basin of the Sarliève marsh, which
133 offered the most dilated, complete, and representative sequence (Fourmont, 2006; Hirschberger et
134 al., 2006; Fourmont et al., 2009). The MDS (*Marais De Sarliève*) cores analyzed in this study were
135 situated between the previous cores S14 and G (see Fig. 1C). The drilling was performed in December
136 2018 using a geotechnical corer on tracks (tubed, 10-cm diameter) for the first 2 m. Between 2 m and
137 5.42 m, a light mechanical corer (Cobra TT, tubed, double cores, 5-cm diameter) was preferred, to
138 avoid compaction of the very ductile sedimentary layers. After being opened, all cores were cleaned
139 and photographed. A selection of the best sections of the cores was used to build the composite core
140 *Marais De Sarliève Composite* (MDSC), on which all the subsequent samplings and analyses were
141 performed. A detailed litho-stratigraphic description was performed in the laboratory.

142 *2.2. Dating and age-depth modeling*

143

144 Considering previous chronological issues, the materials for radiocarbon dating were inspected and
145 selected very carefully. A part of the core between 30 and 505 cm was cut into 2-cm contiguous
146 slices, which were deflocculated in sodium hexametaphosphate and wet sieved at 500 and 100 μm .
147 Both fractions were inspected using a binocular microscope (7.5 \times to 60 \times). Microscopic charcoals and
148 wood or plant fragments were carefully identified with the help of a specialist to avoid aquatic
149 macroremains and any risk of a reservoir effect. One additional dating was performed on fossil pollen
150 extracted from the sediment, following a classical protocol (Brown et al., 1989). After careful
151 microscope inspection by a palaeobotanist, the 80–160- μm fraction (80% *Abies* pollen, 20% residual

152 mineral and organic matter) was selected for dating, which was pure enough to ensure an accurate
153 date (Fletcher et al., 2017). In summary, 12 selected samples were sent to Beta Analytic laboratories
154 for AMS radiocarbon dating (Table 1). Raw dates were calibrated with Calib v.810 and Intcal20
155 (Stuiver and Reimer, 1993; Reimer et al., 2020). A Bayesian age-depth model (BADM) encompassing
156 all the dates was built using Bacon 3.3 (Blaauw and Christen, 2011), keeping the suggested model
157 parameters because previous research suggested a roughly linear accumulation. The sediment
158 accumulation rate was also calculated.

159

160 *2.3 Sedimentology & Geochemistry*

161

162 Coarse fraction samples obtained from sieving 2-cm contiguous slices of core (see above) were
163 examined using a binocular microscope to provide qualitative information on the nature of
164 sediments (e.g., the presence of ostracods, seeds of *Ruppia maritima*, carbonated concretions,
165 pyroclasts). Two half-sections of the MDSC where pyroclasts were identified by this inspection (452–
166 442 and 482–472 cm) were cut and indurated at the EPOC Laboratory (UMR 5805, Bordeaux, F.)
167 using synthetic resin and water-acetone replacement. Micromorphological thin sections were then
168 produced from these blocks following a standard protocol (Guilloré, 1980). Description of the
169 pyroclast facies was performed using a polarizing microscope, allowing a first morphoscopic
170 characterization.

171 Magnetic susceptibility (MS) was measured every 0.5 cm using a Bartington MS2E sensor with high-
172 precision measurements (Dearing, 1999). Sediment for grain-size analysis was sampled every 10 cm
173 and pre-treated following a standard protocol (Fournier et al., 2012). However, samples were not
174 decarbonated to avoid introduction of bias, because carbonates in Sarliève are mainly in the very fine
175 fraction (Fourmont, 2006). Grain-size was then measured with a Malvern Mastersizer 3000 laser

176 granulometer. The results were analyzed using Gradistat (Blott and Pye, 2001). Loss on Ignition was
177 used to estimate organic matter (total organic carbon; TOC) and carbonate (total inorganic carbon;
178 TIC) content in a fraction of the samples used for grain-size, following a two-step protocol (4 hours at
179 550°C, and 2 hours at 950°C) (Heiri et al., 2001).

180 Geochemical analyses were performed using an Avaatech XRF *Core-Scanner* (UMR EDYTEM, F.).
181 Samples were extracted from the MDSC sequence into PVC u-channels, placed in the core-scanner,
182 and covered with an ultrafine film (*ultralene*). Measurements were realized continuously between 8
183 and 539 cm with a resolution of 5 mm. Successive runs using 10 and 30 kV beams generated by a
184 Rhodium anode provided the relative values (in counts per second; cps) of 18 elements (Mg, Al, Si, P,
185 S, K, Ca, Ti, Mn, Fe, Ni, Cu, Zn, Br, Rb, Sr, Zr, Pb). Principal component analysis (PCA) was performed
186 on selected elements using Xlstat to assess relationships between them and the stratigraphic units
187 (Sabatier et al., 2010; Bajard et al., 2015), and to facilitate the selection of elementary ratios as
188 palaeoenvironmental proxies.

189 3. RESULTS

190

191 *3.1 Litho-stratigraphy of the Sarliève marsh*

192

193 A summarized litho-stratigraphic description of the MDSC sequence is presented in Table A.1 (see
194 Appendix A). The stratigraphy is broadly consistent with those described in previous studies,
195 especially with core S14 (Fourmont, 2006), as shown in Fig. 2. However, detailed laboratory
196 inspection revealed new details and some particular sedimentary features (Fig. 2). Seven major
197 stratigraphic units (SUs) were detected, including several subunits and numerous smaller layers. The
198 texture of all the MDSC sequence is clayey and appears quite homogeneous; most differences
199 between layers and SUs concern color and sedimentary features (e.g., laminae).

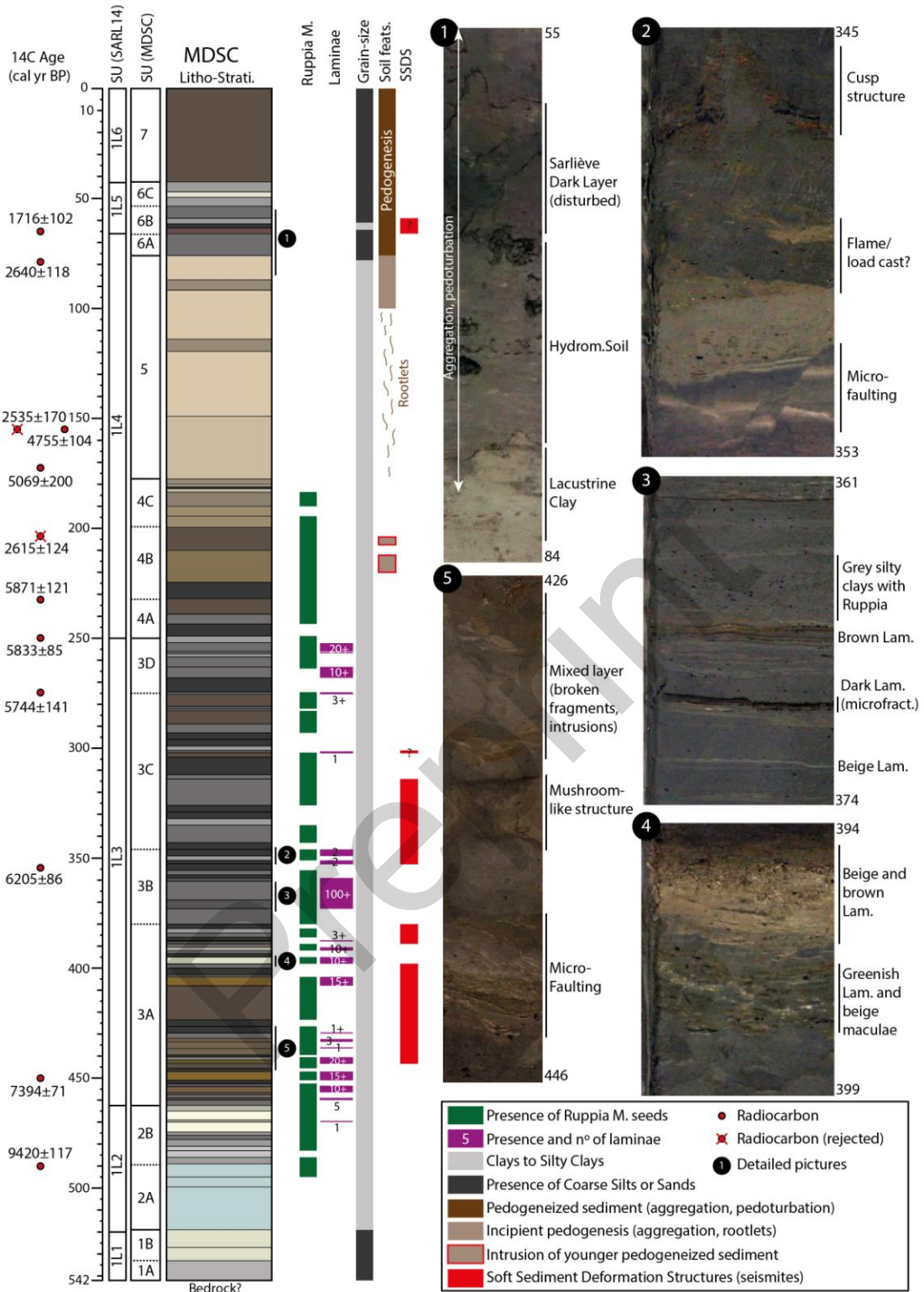
200

201 SU1 (542–519 cm) is characterized by a beige color and a coarser texture, and has arguably been
202 assimilated to surficial deposits or weathered marly substratum in previous studies, whereas SU2
203 (519–462.5 cm) has distinctive bluish and beige colors and a finer grain-size. Its upper half (SU2B)
204 includes the first *Ruppia maritima* seeds in the sequence (Fig. 3E), and has been interpreted in
205 previous works as the onset of a lacustrine brackish body, maintained in overlying units (Fourmont,
206 2006; Fourmont et al., 2009). SU3 (462.5–249 cm) is the thicker unit in the sequence, and is
207 characterized by dark clays with a very marked layering including very abundant *laminae* arranged in
208 bundles (especially SU3A & SU3B, see Figs. 2 and 3C). This SU has been interpreted as abundant
209 detrital inputs under palustrine conditions (dark clay facies), alternating with cyclic water-restriction
210 episodes represented by a characteristic carbonated evaporitic sequence (calcite, dolomite,
211 aragonite) forming the laminations (Bréhéret et al., 2008). The continuous presence of *Ruppia*
212 *maritima* indicates sustained brackish conditions in the SU. We identified a new unit, SU4 (249–177.5
213 cm), which was not described in previous works. This unit is characterized by a brownish color and
214 oxidation features, and the presence of *Ruppia*. SU5 (177.5–76 cm) is certainly the most
215 homogeneous SU in the sequence. It consists of massive beige clays (with some slightly darker layers)
216 of lacustrine origin, as suggested by the presence of abundant aquatic biomarkers such as *characeae*
217 *gyrogonites*, *Daphnia ehippia*, and ostracods (Fig. 3A), consistent with a freshwater body (Fourmont
218 et al., 2009). All the unit exhibits traces of very incipient pedogenesis from upper levels (small
219 rootlets, incipient blocky subangular to angular aggregation above 100 cm, see Fig. 2). SU6 (76–42.5
220 cm) develops from 76 cm, and is a grey clayey hydromorphic soil (pedogenic aggregation, mottles
221 due to pedoturbation) that includes the “Sarliève Dark Layer” (SU6B), which is usually interpreted as
222 a marsh and dated between the Ist and IIIrd c. AD (Vernet, 2005; Vernet et al., 2011). This layer
223 appears manifold and disturbed by post-depositional deformation. SU7 (42.5–0 cm) is the current
224 topsoil.

225 Soft-sediment deformation structures (SSDS) have been detected in several sections of the core, and
226 include abundant micro-faulting of *laminae*, mixed layers with fragments of *laminae* or other layers,
227 mushroom-like structures, bottom-up intrusions of liquefied material, cusp structures, and load casts
228 (Fig. 2). These features are not due to the drilling as they appear in all cores in the same layers,
229 affecting several sedimentary facies with different properties, and were therefore interpreted as
230 seismites (Rodríguez-Pascua et al., 2000; Monecke et al., 2006; Beck, 2009; Shanmugam, 2017). The
231 detected SSDS features can be grouped into five seismic-affected layers (Fig. 2), four of them in SU3
232 (443–398, 389–380, 353–314 and 302–301 cm), and a potential fifth one affecting SU6B (66–59 cm).
233 Following a common stratigraphic approach for the study of seismites in lacustrine deposits, we
234 assumed that each one of these layers was deformed by a major seismic event, which affected
235 unconsolidated sediments from the surface to a certain depth, and normal sedimentation resumed
236 after each event. Therefore, the seismic events can be placed at specific depths in the MDSC
237 sequence, i.e., at the top of each seismic-affected layer (Monecke et al., 2006; Beck, 2009;
238 Stockhecke et al., 2014; Kremer et al., 2017).

239

240

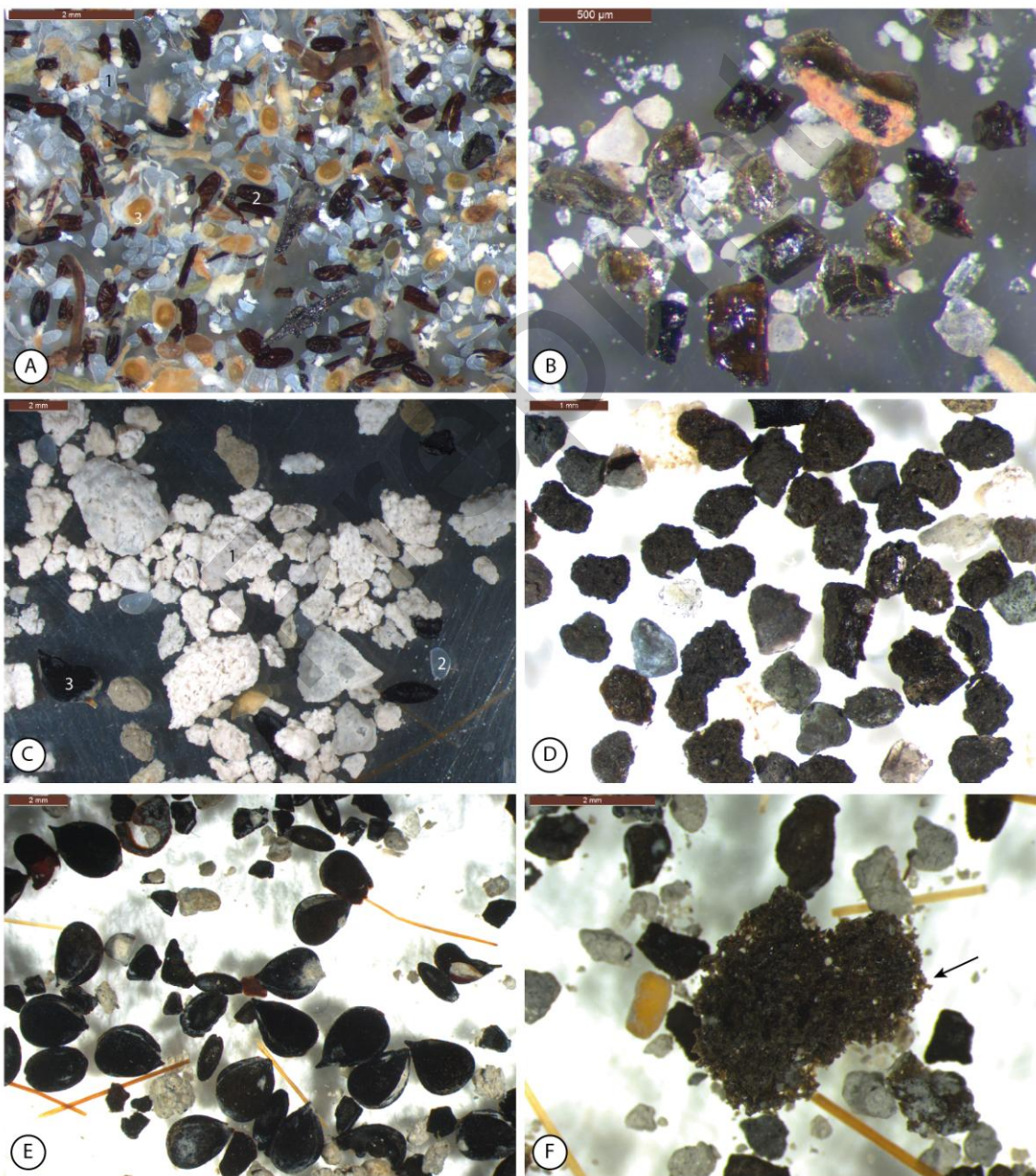


241 **Figure 2.** Litho-stratigraphy, main sedimentary features, and detailed pictures of the MDSC sedimentary
 242 sequence (1–5, note that their position in the sequence is indicated), with the location of 12 radiocarbon dates
 243 (including two that were rejected). The correspondence between SARL14 (Fourmont, 2006) and MDSC (this
 244 study) stratigraphic units (SU) is indicated.

245 Two intrusions of pedogeneized (aggregated) material within the massive and undisturbed sediment
246 of SU4B were detected between 202 and 210 cm (Fig. 2) in the MDSC. This sediment is rich in sands
247 and lithogenic granules, and even includes a microscopic fragment of rusty iron (anthropogenic), and
248 can only be posterior to SU4B. These intrusions are not contaminations during the coring, as they
249 were found at the same depth in different cores. Additionally, a “reworked” layer with very similar
250 features was noted at exactly the same depth in previous drillings close to this point (Ballut, 2000;
251 Fourmont, 2006), indicating that a layer with systematic post-depositional disturbance and intrusion
252 of pedogenized material from above exists between 200 and 210 cm in this sector of the Sarliève
253 basin (see Fig. 2).

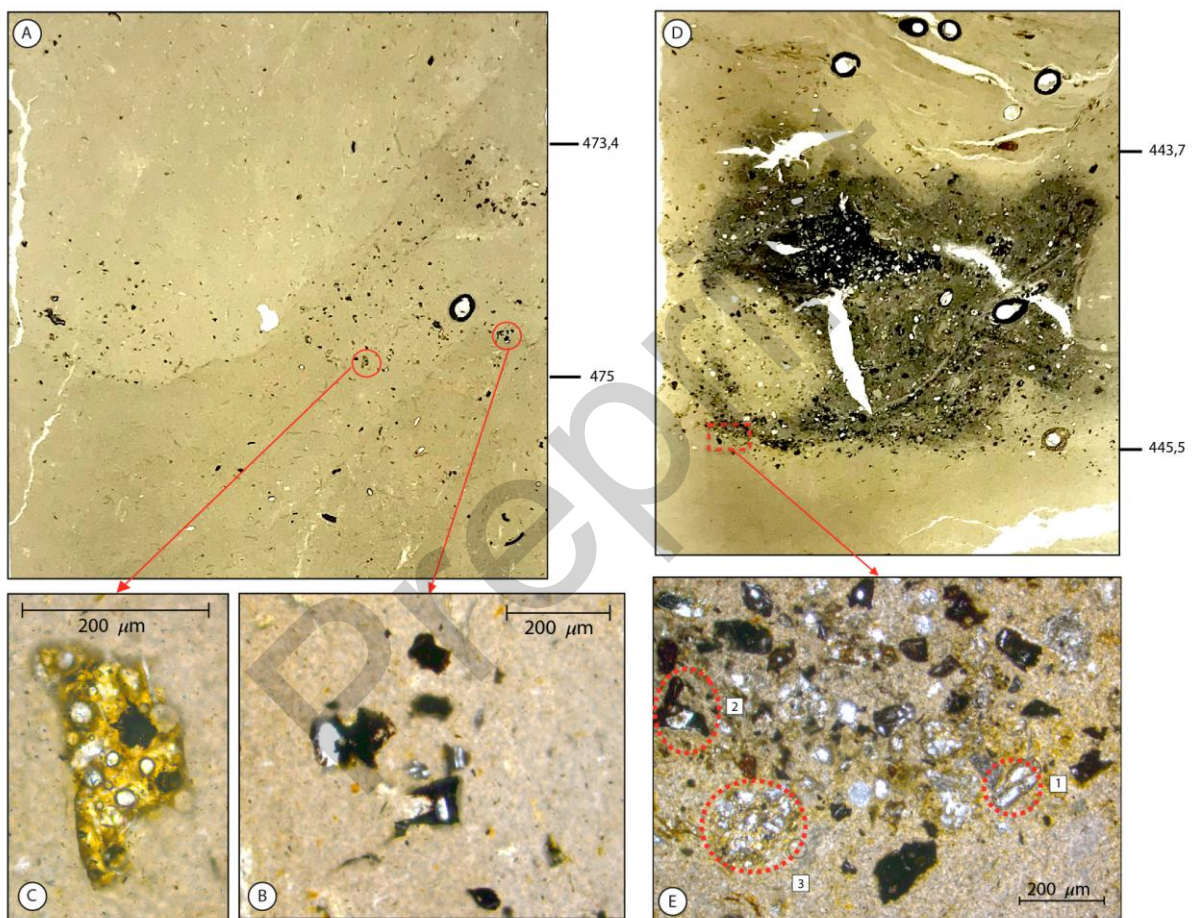
254 Finally, sieving and systematic examination of coarse fractions of the sediment also allowed
255 detection of three layers with high numbers of pyroclasts (Fig. 3B, D & F) at depths of 359, 444–446,
256 and 475–477 cm. The pyroclasts appeared well-sorted, angular, and very sharp, and were certainly
257 not transported by run-off. We interpreted them as (crypto)tephra fallouts in the Sarliève basin,
258 which were hitherto unknown. A preliminary analysis of two of these fallout deposits under the
259 polarizing microscope allowed a first characterization of their facies. Pyroclasts with a size ranging
260 from 30 to 250 μm are visible between 473.4 and 475 cm, being dispersed in the sediment (Fig. 4A, B
261 & C). Between 443.7 and 445.5 cm, pyroclastic material with a similar particle size (50 to 200 μm)
262 forms rather an individualized dark layer (Fig. 4D & E). These two pyroclast-containing deposits have
263 a number of common features: most pyroclasts are angular, with few to no vesicles, and are made of
264 black opaque glass with rare plagioclases and pyroxenes. They are typical of a “blocky morphology”
265 characteristic of phreatomagmatic dynamics (Fisher and Schmincke, 1984; Heiken and Wohletz,
266 1985; Cas and Wright, 1987; Bourdier et al., 1994). In both cases, bigger (200 μm) light-brownish
267 pyroclasts made of translucent glass are less frequent. They show a pumice-like high density of
268 vesicles (Heiken and Wohletz, 1985), and indicate more magmatic phases during the corresponding
269 eruption (Fig. 4C & E). The fine fraction ($>50 \mu\text{m}$) of the 473.4–475 cm deposit also contains shard-
270 like vitric pyroclasts (black opaque glass). These are likely to have been formed during the cooling

271 and fragmentation phase of a phreatomagmatic eruption. Between 443.7 and 445.5 cm, free mineral
272 shards in a glassy matrix with more or less vesicles (bubble-wall texture; Fisher, 1963) can be
273 observed (Fig. 4E). The “fresh” aspect of the pyroclasts in both deposits confirms that they are *in situ*
274 tephra fallouts, and their morphology points clearly to origins in eruptions with phreatomagmatic
275 phases. As the majority of the eruptions in the neighboring Chaîne des Puys have had such phases,
276 further geochemical analysis (e.g., electron microprobe) is necessary to facilitate detailed discussion
277 of the origin of these tephtras.



278

279 **Figure 3.** Selected samples of the coarse fraction of the sediment (500 μm) after wet sieving. A) 172–174 cm:
 280 markers of freshwater lacustrine conditions (ostracods [1], *characeae* gyrogonites [2], ehippia of *Daphnia* [3]),
 281 microcharcoal and organic debris; B) 359 cm: angular volcanic minerals, one of them embedded in reddish
 282 scoria, of pyroclastic origin; C) 394–396 cm: beige carbonated concretions from a lamination (1), a few
 283 ostracods (2), and *Ruppia maritima* seeds (3); D) 444–446 cm: dark, angular, and well-sorted scoriaceous
 284 pyroclasts; E) 463–465 cm: *Ruppia maritima* seed concentration; F) 475–477 cm: big scoriaceous pyroclast with
 285 vesicular texture and sharp edges (black arrow)



286

287 **Figure 4.** Macro- (A & D) and microphotographs (B, C & E, PPL) of the layers containing pyroclasts at 473.4–475
 288 (A, B, & C) and 443.7–445.5 cm (D & E) in the MDSC sequence. A) Pyroclasts dispersed in sediment; B) glassy
 289 opaque pyroclasts, angular; C) brownish glassy pyroclasts, with abundant vesicles (pumice-like); D) well-
 290 individualized dark pyroclastic layer; E) (1) free mineral shards in a glassy gangue with more or less vesicles; (2)
 291 glassy opaque pyroclasts, angular; (3) brownish glassy pyroclasts with abundant vesicles (pumice-like).

292 3.2 Chronology and age-depth model

293

294 The results of the radiocarbon dating are summarized in Table 1. The dates range from 1716±102 cal
295 yr BP (65 cm) to 9420±117 cal yr BP (c. 490 cm). All of the dated samples have $\delta^{13}\text{C}$ values consistent
296 with terrestrial materials, and therefore a reservoir effect from old carbonates is not likely. Of the 12
297 dates, 10 are in normal stratigraphic order. Date 6 (terrestrial plant material, 202–206 cm) is clearly
298 outlying, as it is in marked chrono-stratigraphic inversion to the surrounding dates of samples 5 and 7
299 (charcoal). However, the significantly younger age of sample 6 is consistent with an intrusion of
300 pedogenic sediment from upper levels (see above). Date 6 was therefore rejected from a
301 stratigraphic perspective, but is considered in the discussion. The situation is slightly more complex
302 for dates 3 (wood fragment) and 4 (pollen), which were performed on samples from the same depth
303 (154–156 cm). Date 4 is consistent with dates 2 and 5; however, date 3, although not inconsistent
304 with date 5, is significantly younger than date 4, and is in chronological inversion with date 2
305 (charcoal). Date 3 would also imply a period of very slow sedimentation rate after date 5, followed by
306 a quasi-instantaneous deposition of sediment between dates 2 and 3 (c. 80 cm of sediment), which is
307 not consistent with the nature of the sediment (see description). Additionally, the woody material
308 used for date 3 could be from rootlets, which are relatively abundant in this section of the core (see
309 litho-stratigraphic description and Fig. 2). Therefore, date 3 probably represents the age of terrestrial
310 soils from upper levels. In contrast, date 4 was performed mostly on *in situ* *Abies* pollen, which was
311 well preserved and with no signs of reworking. On the basis of these arguments, we rejected date 3
312 in favour of date 4 for the 154–156 cm level. Remarkably, dates 2, 3, and 6 are almost the same,
313 suggesting that they all could be due to incipient (but deep) pedogenesis phenomena (e.g.,
314 aggregation and cracking with fall of micro-aggregates, intrusion of rootlets or burrowing by micro-
315 to macrofauna) related to the development of a hydromorphic soil from around 76 cm (i.e., circa
316 date 2) to the current surface.

317

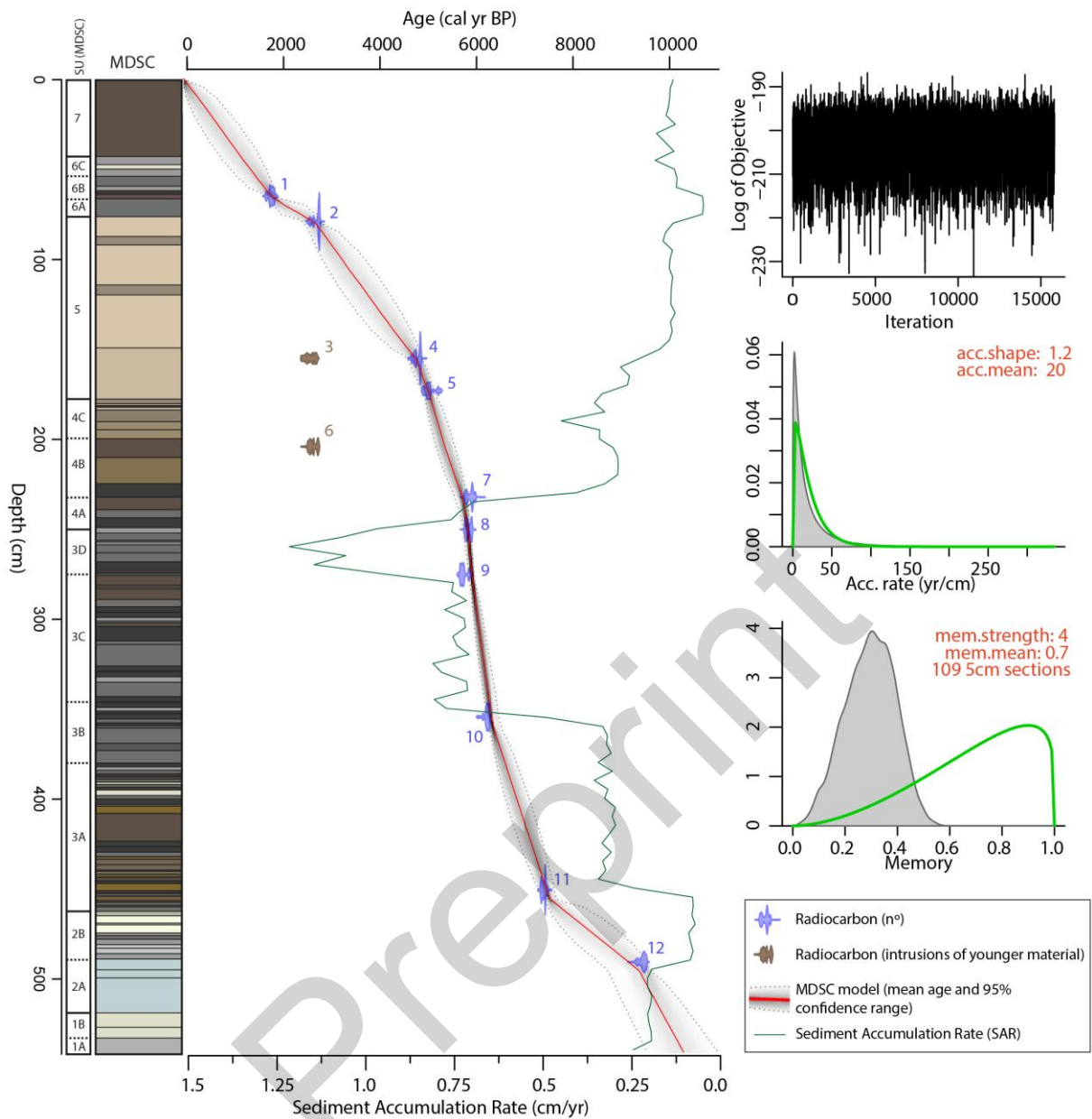
318

Table 1. Radiocarbon dates from the MDSC core. Dates in *italic* were rejected (see the text).

No.	Core	Depth (cm)	Lab Code	Material	$\delta^{13}\text{C}(\text{o/oo})$	^{14}C yr BP	Cal yr BP	Cal yr BP (median, 2σ)	Cal yr BCE/CE (median, 2σ)
1	MDSC	64–66	Beta-526086	Charcoal	-24.0	1810±30	1819–1614	1716±102	234±102 CE
2	MDSC	78–80	Beta-532571	Charcoal	-24.3	2580±30	2758–2522	2640±118	690±118 BCE
3	<i>MDSC</i>	<i>154–156</i>	<i>Beta-527734</i>	<i>Wood</i>	<i>-25.3</i>	<i>2460±30</i>	<i>2706–2365</i>	<i>2535±170</i>	<i>585±170 BCE</i>
4	MDSC	154–156	Beta-546604	Pollen	-26.0	4240±30	4860–4651	4755±104	2805±104 BCE
5	MDSC	172–174	Beta-536397	Charcoal	-25.9	4420±30	5270–4869	5069±200	3119±200 BCE
6	<i>MDSC</i>	<i>202–206</i>	<i>Beta-532573</i>	<i>Plant material</i>	<i>-26.4</i>	<i>2520±30</i>	<i>2738–2493</i>	<i>2615±124</i>	<i>665±124 BCE</i>
7	MDSC	230–234	Beta-536396	Charcoal	NA	5140±40	5992–5750	5871±121	3921±121 BCE
8	MDSC	249–251	Beta-520489	Charcoal	NA	5100±30	5919–5748	5833±85	3883±85 BCE
9	MDSC	274–276	Beta-532574	Charcoal	-23.0	4990±30	5885–5603	5744±141	3794±141 BCE
10	MDSC	353–355	Beta-526088	Charcoal	NA	5410±30	6291–6119	6205±86	4255±86 BCE
11	MDSC	449–451	Beta-520490	Plant material	-27.6	6490±30	7465–7323	7394±71	5444±71 BCE
12	MDSC	484–496	Beta-527735	Charcoal	NA	8440±60	9538–9303	9420±117	7470±117 BCE

319

320 All dates (n=12) were used for the Bayesian age-depth modeling. The resulting BADM is presented in
321 Fig. 5, including the mean age (used for discussion), 95% confidence interval, and accumulation rate.
322 The confidence interval ranges from 1500 years (worse, base of the core) to 100 years (best, date 9).
323 More than 15,000 stored iterations show a rather stable run with a stationary distribution. Dates 3
324 and 6 appear too young, and are bypassed by the Bayesian model, which is consistent with previous
325 assessments and reinforces the hypothesis of contamination by pedogenetic processes from upper
326 levels. The base of the model is interpolated and provides an age range of 9494–10,996 cal yr BP
327 (mean of 10,285 cal yr BP) at 540 cm; however, this is uncertain because the lower date (12) is
328 vertically imprecise (484–496) at the boundary between SU2A and SU2B. Therefore, the chronologies
329 of the units underlying SU2A, and especially SU1, are uncertain because a sedimentary hiatus cannot
330 be discarded. The sediment accumulation rate (SAR, see Fig. 5) is generally low at the base and the
331 top of the core (SU1-2 and SU4B-7), but rises in SU3A and 3B, and peaks strongly in SU3C and
332 SU3D/4A.



333

334

Figure 5. Bayesian age-depth model (BADM) of the MDSC sequence and sediment accumulation rate in

335

cm/year, built with Bacon 3.3 using the default recommended parameters for prior distribution for

336

accumulation rate and memory. Iterations show a rather stationary distribution.

337

338

339

340

341 *3.3 Sedimentological data*

342

343 Sedimentological data for SU1–6 are summarized in Figure 6. Binocular microscope inspection of
344 several pre-treated samples showed that besides clay and silts, there were also some fragments of
345 ostracods and mica sheets (c. 100–300 μm) and a few coarser quartz grains (>500 μm).

346 The sediment in SU1 appears to be mainly composed of clays and fine to medium silts (main mode at
347 2–7 μm , with a significant presence of silts and sands up to 300 μm). The sand content is
348 nevertheless higher than 5%, with a very high D90 and a very low D50, indicating relatively poor
349 sorting. The unit also has the highest TIC and lowest TOC contents of the whole sequence. Taken
350 together, these data suggest a very mineral nature to the sediment, close to natural marly bedrock,
351 and a colluvial transport process.

352 SU2A is relatively similar, but with slightly lower TIC and higher TOC, and much less sands and much
353 lower D90, suggestive of better sorting. SU2B is characterized by a slight increase in the clay content,
354 reappearance of sands (rise of D90), and a marked decrease in TIC, while TOC peaks strongly at c.
355 30%. However, this TOC increase is unlikely caused by a massive increase in organic carbon content,
356 as it is not reflected at all in the sediment aspect (see description). The TOC peak in SU2B is most
357 probably due to thermal decomposition of magnesium carbonates (Heiri et al., 2001), especially
358 abundant in SU2 (Fourmont, 2006; Fourmont et al., 2009). Grain size diagrams show bimodal
359 distributions in SU2, with dominant modes at 10–25 μm in SU2A and 1–4 μm in SU2B (Fig. 6). Minor
360 modes appear at c. 100 (fragments of ostracods) and 1000 μm (coarse sands). The MS signal is
361 almost flat, although a small peak at 475 cm coincides with the presence of pyroclasts detected
362 during the inspection of the coarse fraction (Fig. 3F, Fig. 4A–C), indicating the presence of a
363 cryptotephra. In general, the sedimentological data suggest a change in sedimentary conditions from
364 the opening of SU2 towards a lower energy sedimentary environment, with some higher energy

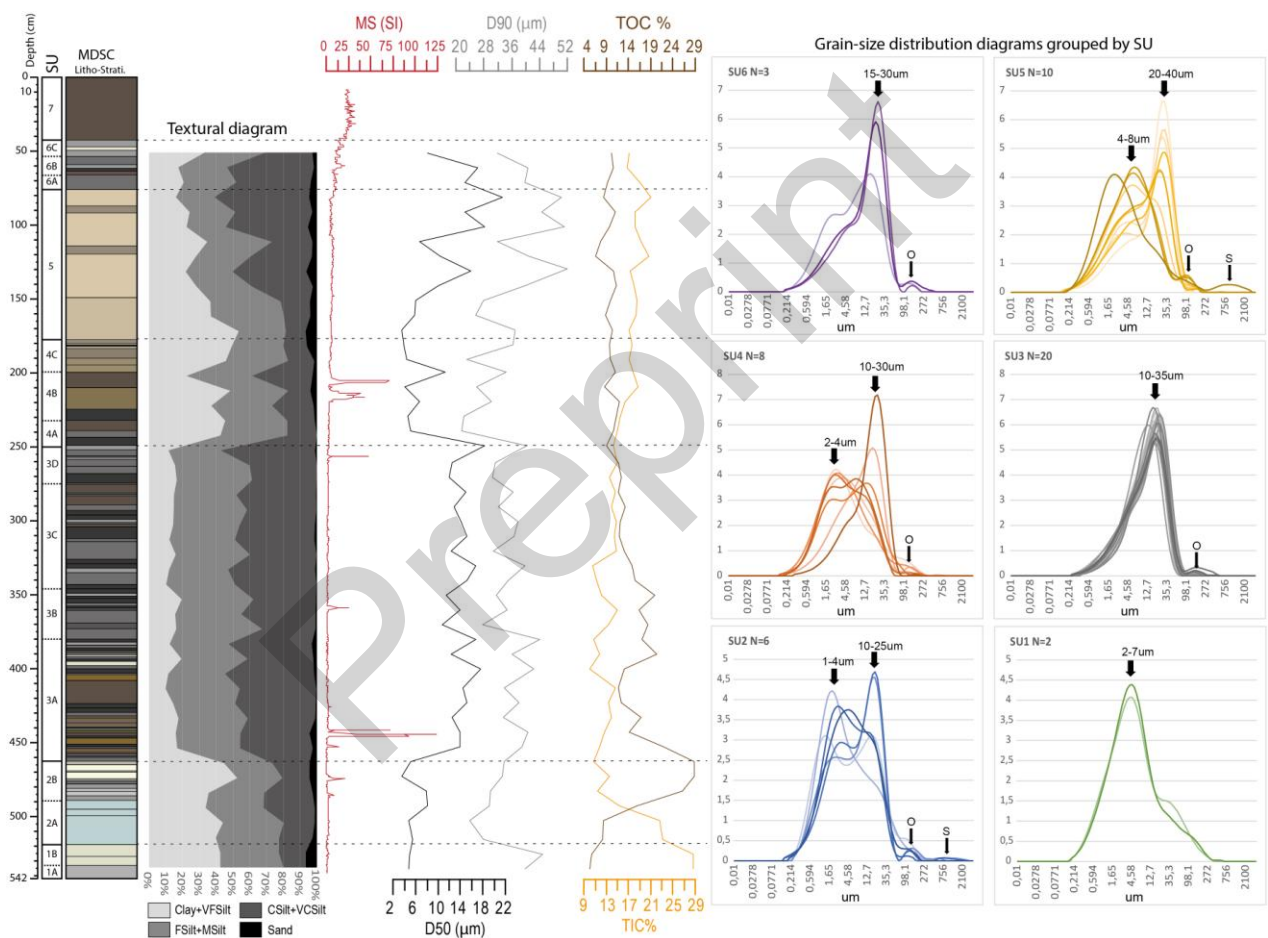
365 sedimentary inputs, consistent with a small water body rich in calcium (SU2A) and magnesium (SU2B)
366 carbonates.

367 The textural features of SU3 are significantly different to those of SU2: the clay content shows a
368 sharp decay, and the sediment is largely and consistently dominated by silts (80%–90%). Sands
369 become quickly negligible after the base of SU3A. D50 and D90 are very similar, indicating very good
370 sorting, and are roughly constant in all of SU3. Grain-size diagrams are unimodal (c. 10–35 μm , a
371 small peak at approximately 160 μm is due to fragments of ostracods) and virtually identical for all
372 the samples (n=20). TIC is also relatively low and constant (10%–15%), with very limited fluctuations,
373 suggesting limited carbonate inputs or precipitation. TOC falls significantly after the SU2B peak, and
374 remains between 12%–15%, with an upwards trend to reduction (except for SU3B, where it reaches
375 values of c. 20%, suggesting a more OM-rich wetland environment). The sedimentological data
376 indicate a homogeneous sedimentary environment in terms of transport processes in all the SU,
377 suggesting a very efficient sorting mechanism quasi-limited to the silt fraction, *a priori* alluvial or
378 aeolian. However, in such a small catchment alluvial processes alone would not have been enough to
379 produce that extremely good sorting. Additionally, only anecdotal aeolian deflation processes
380 related to modern cropping have been documented in the Limagne (Barathon and Valleix, 1993).
381 Furthermore, the quasi absence of clays is surprising in the depocenter of a rather flat endorheic
382 basin (Bréhéret et al., 2003; Fourmont et al., 2009; Macaire et al., 2010). This suggests that the
383 sedimentary features of SU3 are rather inherited from a silt-sized, very homogeneous and well-
384 sorted source of sediment, which is *a priori* not evident within the soils and rocks of the catchment.
385 The MS shows at least four peaks: at 452.5, around 441–444.5, at 359, and at 256.5 cm. All are very
386 sharp and stand out against the low background signal. Moreover, two of them (at 444.5 and 359
387 cm) coincide with pyroclasts detected under the binocular microscope (Fig. 3B & 3D, Fig. 4D & E). The
388 four MS peaks are therefore probably indicative of cryptotephra fallouts.

389 The texture becomes finer again in SU4, with much more clays (40–50%) and up to 40% fine to
390 medium silts. This indicates a sedimentary environment with much less energy than SU3. Sands are
391 absent in SU4A, but their content increases upwards in SU4B and 4C. D50 and D90 are lower
392 throughout than in SU3, and have quite different trends, indicating relatively poor sorting. Grain-size
393 diagrams show two modes at 2–4 μm and 10–30 μm without any clear upwards trend, and also a
394 small peak at 100–160 μm corresponding to ostracod fragments and fine sands. TOC is maintained at
395 about 10%, and TIC increases gradually from 11% to 16% upwards, indicating more consistent
396 precipitation of carbonates or detrital influx. MS exhibits two big peaks clearly associated with the
397 pedogenic intrusions in SU4B (see description and Fig. 2). Although difficult to interpret from these
398 data alone, SU4 appears similar to SU2 from a sedimentological perspective, and could therefore be
399 consistent with a low-energy small waterbody with higher energy inputs towards the top of the unit.

400 Textural diagram and grain-size indicators show a very clear upwards trend to coarsening in SU5. The
401 clay content falls through the unit from 50% at its base to c. 20% at its top, and is replaced by coarse
402 and very coarse silts from c. 150 cm (from 15% to c. 50%), whereas fine silts and sands maintain their
403 respective weights. D50 and D90 covary, and show the same marked trend to coarsening. A first
404 rising phase from the base of the SU culminates in a strong peak in grain-size at c. 130 cm. Two other
405 peaks (c. 100 and 80 cm) are separated by lower values at c. 110–120 and 90 cm, coincident with
406 darker layers. Grain-size diagrams clearly reflect the coarsening-upward trend, with a mode of c. 4–8
407 μm for samples in the lower part of SU5, shifting gradually to 20–40 μm for samples in its upper part.
408 Small peaks appear at 100–160 μm (ostracod fragments and fine sands) and above (coarser sands).
409 TOC remains stable at around 10%, whereas TIC rises slowly from 15 to 19%. Sedimentological data
410 show a clear pattern of coarser (but relatively well-sorted) sedimentary inputs in an otherwise low-
411 energy environment, probably lacustrine and carbonated (see description, Figs. 2 and 3). This pattern
412 appears consistent with the increased soil erosion suggested by previous studies of this phase
413 (Macaire et al., 2010), and growing sedimentary inputs transported by diffuse to concentrated
414 runoff, with short phases of relatively reduced sedimentary energy.

415 Textural and grain-size diagrams of SU6 indicate a composition very similar to the top of SU5, i.e.,
 416 dominated by silts and coarse silts. However, the D50 and D90 show an incipient trend to grain-size
 417 reduction towards the top of the unit. TIC and TOC maintain values of c. 15% and 10% respectively.
 418 Increased and maintained MS values are consistent with the pedogenic aggregation and the
 419 pedoturbation noted in the description, and indicate soil development (Fig. 2, Table A.1). These data
 420 confirm that SU6 is the pedogenized top of SU5, with the reduction in coarser detrital inputs being
 421 probably due to a loss of sedimentary connectivity in what is now a terrestrial environment.



422
 423 **Figure 6.** Selected sedimentological results of the MDSC core. Black arrows in the grain-size distribution
 424 diagrams indicate the main modes. For each diagram, the hues of the curves are lighter towards the top of the
 425 unit. MS: magnetic susceptibility ($Si \cdot 10^{-5}$), TOC: total organic carbon, TIC: total inorganic carbon, O: ostracods, S:
 426 sands, SU: stratigraphic unit, N: number of samples. Sizes are in micrometers (μm). Horizontal dashed lines:
 427 main SU limits.

428 *3.4 Geochemical proxies*

429

430 Results of the XRF elementary analysis are reported in Fig. 7. The PCA shows a rather well separated
431 dataset with F1 and F2 (PC1 and 2) accounting for 54% and 15% of the variance respectively (Fig 7B).
432 Two major clusters of elements are clearly distinguished: the first cluster groups almost all the
433 terrigenous elements with positive loadings on F1, and a second one includes carbonate-related
434 elements (Ca, Sr, and Mg) with positive loadings on F2. Finally, Pb and S appear isolated and
435 independent of the two mentioned poles.

436 All terrigenous elements show a roughly similar signal, and carbonate related-elements (Ca, Sr, Mg)
437 also share a common trend throughout the sequence (Fig. 7A). However, S and Pb show different
438 behaviors with several peaks unrelated to the other elements in MDSC.

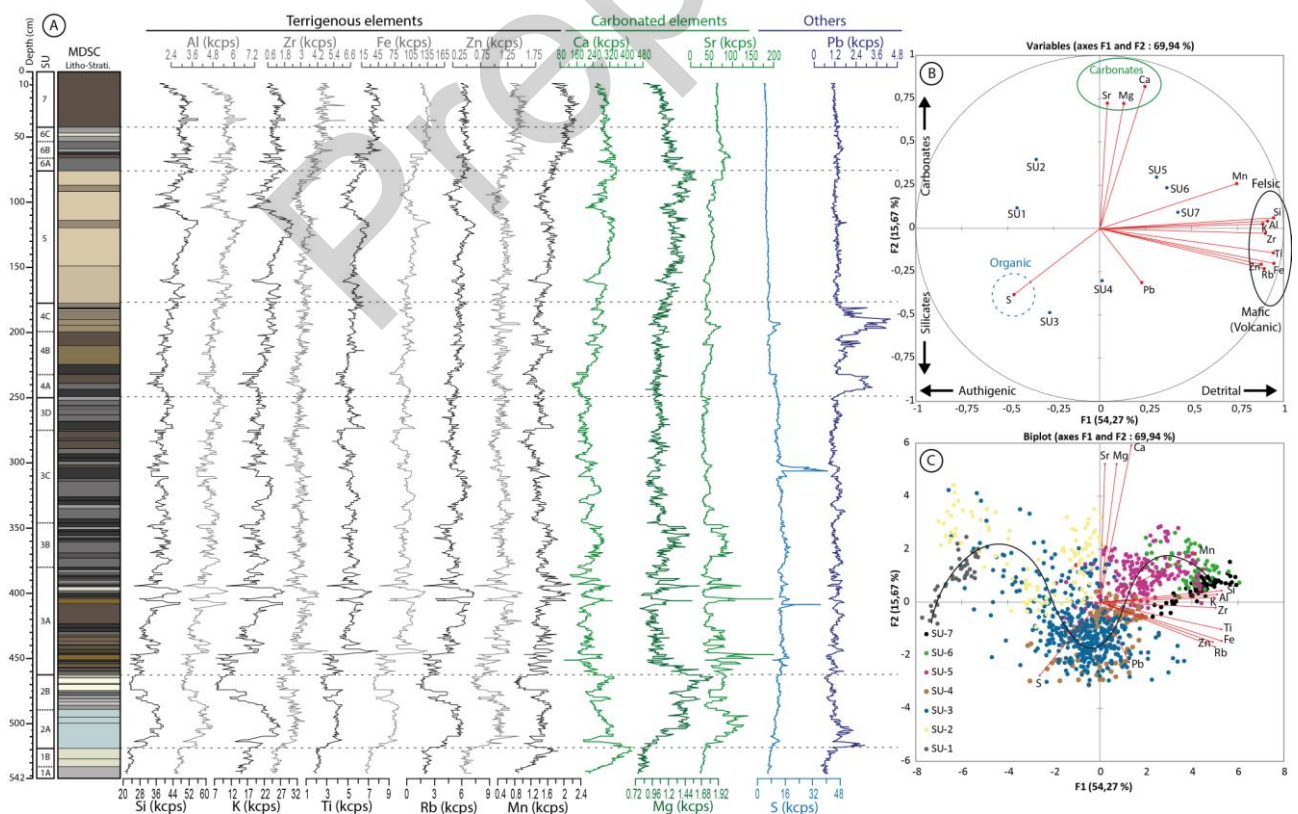
439 Following the positions of the different SUs in the PCA (Fig. 7B & C) and considering their
440 characteristics and the previous sedimentological information, we interpreted F1 as a balance
441 between detrital and authigenic influx in the basin: higher loadings represent increased detrital
442 inputs from the catchment, including volcanic, siliceous, carbonated, and mixed materials, whereas
443 neutral to negative loadings are rather interpreted as dominant authigenic processes such as
444 chemical or evaporitic precipitation during periods of low hydro-sedimentary inputs. On the basis of
445 the available detailed geochemical characterization of the catchment (Fourmont, 2006; Fourmont et
446 al., 2009), it appears that F2 clearly reflects geochemical sourcing: carbonates have positive loadings,
447 whereas silicates, including minerals from felsic and mafic/volcanic rocks, have neutral and negative
448 loadings respectively (Fig. 7B). The biplot (Fig. 7C) shows a clear geochemical progression in the
449 MDSC sequence: SU1 and 2 are dominated by authigenic carbonates in low detrital input conditions;
450 SU3 and 4 are characterized by increased detrital inputs of rather siliciclastic and volcanic materials;
451 and SU5 and 6 have even higher detrital contributions, with again the dominance of carbonated
452 materials. These trends are consistent with what is known about the nature of different SUs in the

453 Sarliève marsh (see introduction), and with sedimentological data and descriptions (Table A.1, Figs. 2,
454 3, and 6).

455 On the basis of the results of the PCA, litho-stratigraphy, sedimentological data, and considering
456 geological characteristics of the study area (see introduction), we selected several elementary ratios
457 to use as palaeoenvironmental proxies. Previous studies demonstrated that authigenic aragonite
458 formed during evaporitic events in the Sarliève marsh (Bréhéret et al., 2008). As Sr is more abundant
459 in evaporitic aragonite than in other carbonate minerals (Salminen et al., 2005), the Sr/Ca ratio can
460 here be used as a proxy of evaporitic conditions. Mn has a strong sensitivity to variability in redox
461 conditions, specifically to dryer phases in otherwise wet environments (Kylander et al., 2011).
462 Knowing that Fe has an opposite sensitivity, we used high values of Fe/Mn, a typical redox indicator
463 (e.g., Cuven et al., 2011), as a proxy of change towards reducing (poorly oxygenated) conditions,
464 including saturated soil/marsh phases (Lindbo et al., 2010). Considering the PCA distribution and the
465 fact that volcanic materials are usually richer in Fe (Salminen et al., 2005), the Fe/Si ratio is
466 interpreted as an overall indicator of fine volcanic sediment from the catchment (e.g., Van Daele et
467 al., 2014). However, we propose to also use it as an indicator of basaltic cryptotephra, which should
468 cause sharp increases in relative Fe content.

469 The background S signal can be interpreted as increased OM content, occurring mostly in SU3 (dark
470 color, strong H₂S smell), and is closely related to Pyrite in continental wetland environments under
471 anoxic conditions (Salminen et al., 2005). A minor contribution to the S signal could also come from
472 gypsum; however, there is only marginal content in the Sarliève sediments (Fourmont, 2006). In
473 contrast, sharp spikes are not explained by these sources; therefore, sudden increases of S can only
474 be explained by volcanic activity. Volcanos can produce massive injections of SO₂ into the
475 atmosphere, which is detectable in sediment and ice cores (e.g., Dunbar et al., 2017; Baldini et al.,
476 2018). We therefore propose interpreting the two unusually sharp S spikes at 410 and 305 cm as
477 particularly intense volcanic degassing episodes.

478 The Pb content is poorly explained by the PCA, suggesting that it is not related to detrital or
 479 authigenic minerals. Moreover, there is not a natural Pb source within the lithology of the catchment
 480 (Fig. 1). Anthropogenic sources elements can also be discarded: the Pb peaks (515–520, 505–508, 230–250,
 481 and 180–200 cm) are older than the first traces of metallurgy in western Europe, which occurs at c.
 482 5000 cal yr BP (Carozza et al., 2015; Martínez Cortizas et al., 2016). Additionally, the total absence of
 483 later peaks suggests that these Pb-enrichments are more related to time-constrained events rather
 484 than to a regular source such as the catchment or human activities. The most likely source is
 485 therefore volcanic activity, which produces significant amounts of Pb through degassing or volcanic
 486 ash leaching (Witham et al., 2005; Kylander et al., 2010; Ayris and Delmelle, 2012). The Pb is then
 487 transported by runoff and fixed in sedimentation areas. Considering the thickness of the Pb-enriched
 488 sections of the core, long-term ash leaching seems far more plausible than punctual degassing.
 489 Therefore, we used the Pb/Rb ratio to distinguish these volcanic Pb inputs from background content
 490 (see Fig. 9).



491

492 **Figure 7.** Selected geochemical results of the MDSC core. A) Elementary data (cps: counts per second); B) PCA
493 correlation circle according to factors F1 and F2, with identified clusters of elements and positions of SUs; C)
494 plot with distribution of measurements by SU (black sinusoidal arrow: global trajectory of the basin).

495

496 4. DISCUSSION

497

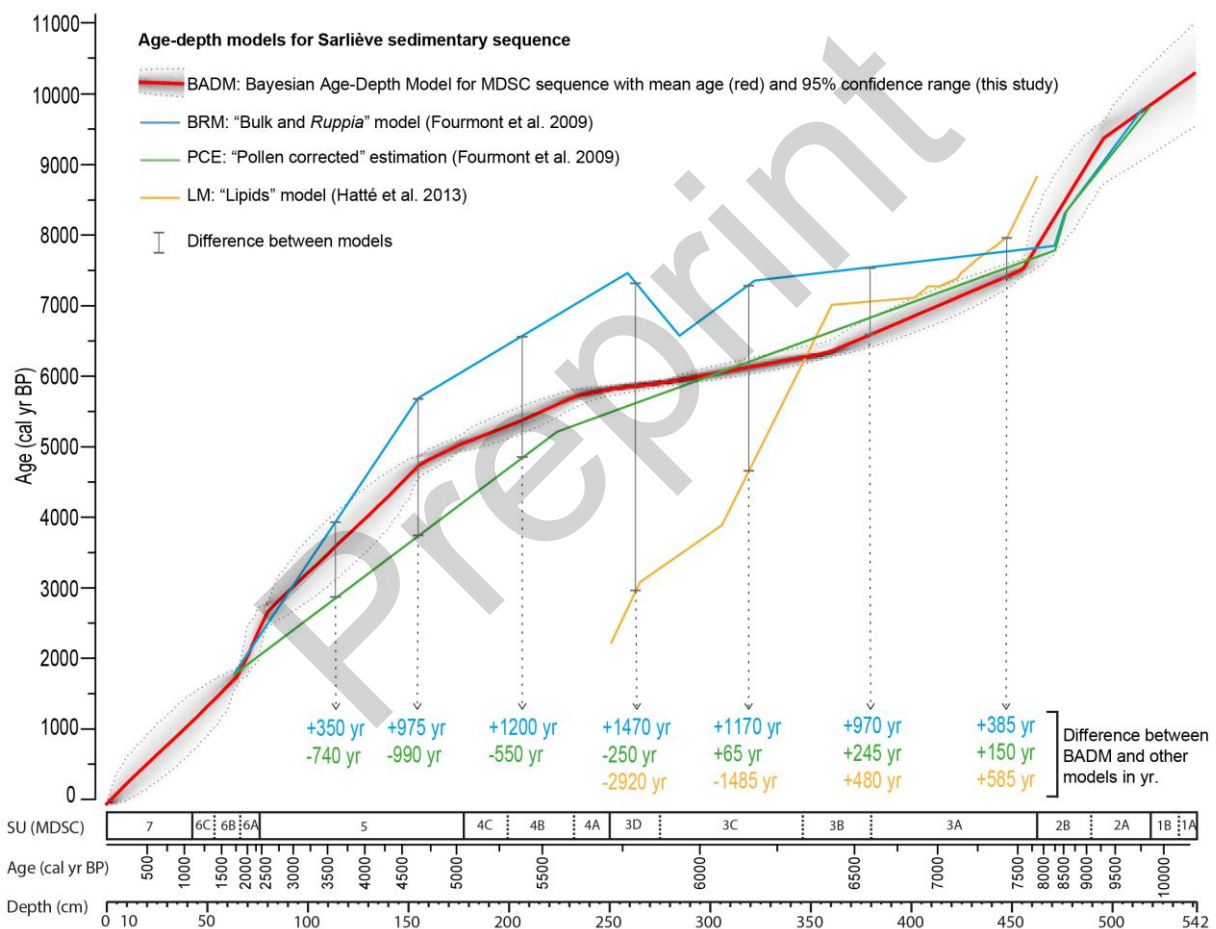
498 *4.1 Changing times: an improved chrono-stratigraphy for the Sarliève sedimentary* 499 *sequence*

500

501 Three chronologies for the sedimentary infilling of the Sarliève basin were published between 2009
502 and 2013 (see introduction for details): the “Bulk and Ruppia” or BRM model, the “pollen-corrected
503 estimation” — PCE — model (both in Fourmont et al., 2009), and the “lipids model” — LM (Hatté et
504 al., 2013). From its first publication, the BRM appeared aged: the dated materials were mainly
505 carbonated bulk sediment and *Ruppia maritima* seeds, introducing important and uncontrolled
506 ageing into the age-depth model (Yansa and Long, 2007; Grimm et al., 2009). The PCE model, based
507 on the regional palynozones, was then proposed as a younger and more reliable chronological
508 framework (Fourmont et al., 2009). This approach implied several major inconveniences: first, the
509 ages were only estimated; second, the palynozones were extrapolated from mountain areas of the
510 Massif Central, although they are still unclear in the Limagne lowlands; third, it prevented an
511 independent discussion of the chronology of the palynological data. Later works tried to rectify part
512 of the age-depth model (only SU3) by dating lipids (Hatté et al., 2013); however, this led to a
513 significantly younger and controversial chronology that was extremely inconsistent with the regional
514 vegetation history (Miras, 2016). In contrast, the Bayesian age-depth model (BADM) produced in this
515 study is based on carefully selected organic materials for radiocarbon dating, such as charcoal and

516 plant/wood remains, and is therefore considered more accurate than the previous models with
 517 which it is compared (Fig. 8).

518 The differences detected between the old models and the new more-accurate BADM proposed in
 519 this work are very significant in SU3, 4 and 5 (roughly 7500-2500 cal yr BP, see Fig. 8), with positive
 520 and negative offsets up to 1000 (PCE), 1500 (BRM) and even 3000 years (LM). This implies that the
 521 sequence may be subject to a substantial chronological revision and a palaeoenvironmental
 522 reinterpretation, which is addressed in the following parts of the discussion.



523

524 **Figure 8.** Graphical comparison between the different age-depth models for the Sarliève marsh sedimentary
 525 sequence.

526

527

528 *4.2 New insights into Early and Middle Holocene volcanic phenomena*

529

530 Figure 9 summarizes sedimentological, geochemical, and litho-stratigraphic indicators of Holocene
531 volcanic phenomena (see previous sections) recorded in the Sarliève marsh. Six potential (crypto)
532 tephra layers (T1 to T6) were identified on the basis of MS, Fe/Si, and the presence of pyroclasts in
533 500 and/or 100- μm sieve residues. Five of these tephra layers had not been detected in previous
534 works (see introduction), highlighting the fundamental contribution of multi-proxy and high
535 resolution analysis for detecting cryptotephra. The absence of pyroclasts when other proxies
536 suggest the presence of tephras is not definitive, and will be checked by further studies, as particles
537 below 100 μm were not examined in this work. The presence of T1 (c. 9750 cal yr BP) is very likely, as
538 it is marked by a major spike in Fe/Si and a small spike in S (Fig. 9). T2 (c. 8500 cal yr BP) is more
539 tangible thanks to the presence of some pyroclasts (Fig. 3F, Fig. 4A–C) and high MS values. T3 (c.
540 7500 cal yr BP) is a more uncertain level, but sharp peaks in MS and Fe/Si are strongly suggestive of
541 the presence of a cryptotephra. T4 (c. 7400 cal yr BP) is certainly the clearest volcanic fallout in the
542 sequence, because abundant pyroclasts (Figs. 3D, 4D, & E) coincide with strong and very sharp peaks
543 of Fe/Si and MS. T5 (c. 6300 cal yr BP) is also supported by the presence of pyroclasts (Fig. 3B) and an
544 MS peak. Finally, the T6 fallout (c. 5800 cal yr BP) is strongly suggested by a distinctive MS peak, but
545 the apparent lack of other coinciding indicators means that further analysis is required for
546 confirmation. Two degassing events are indicated by very sharp spikes in the S curve that are well-
547 detached from the background signal at c. 6950 and 6050 cal yr BP.

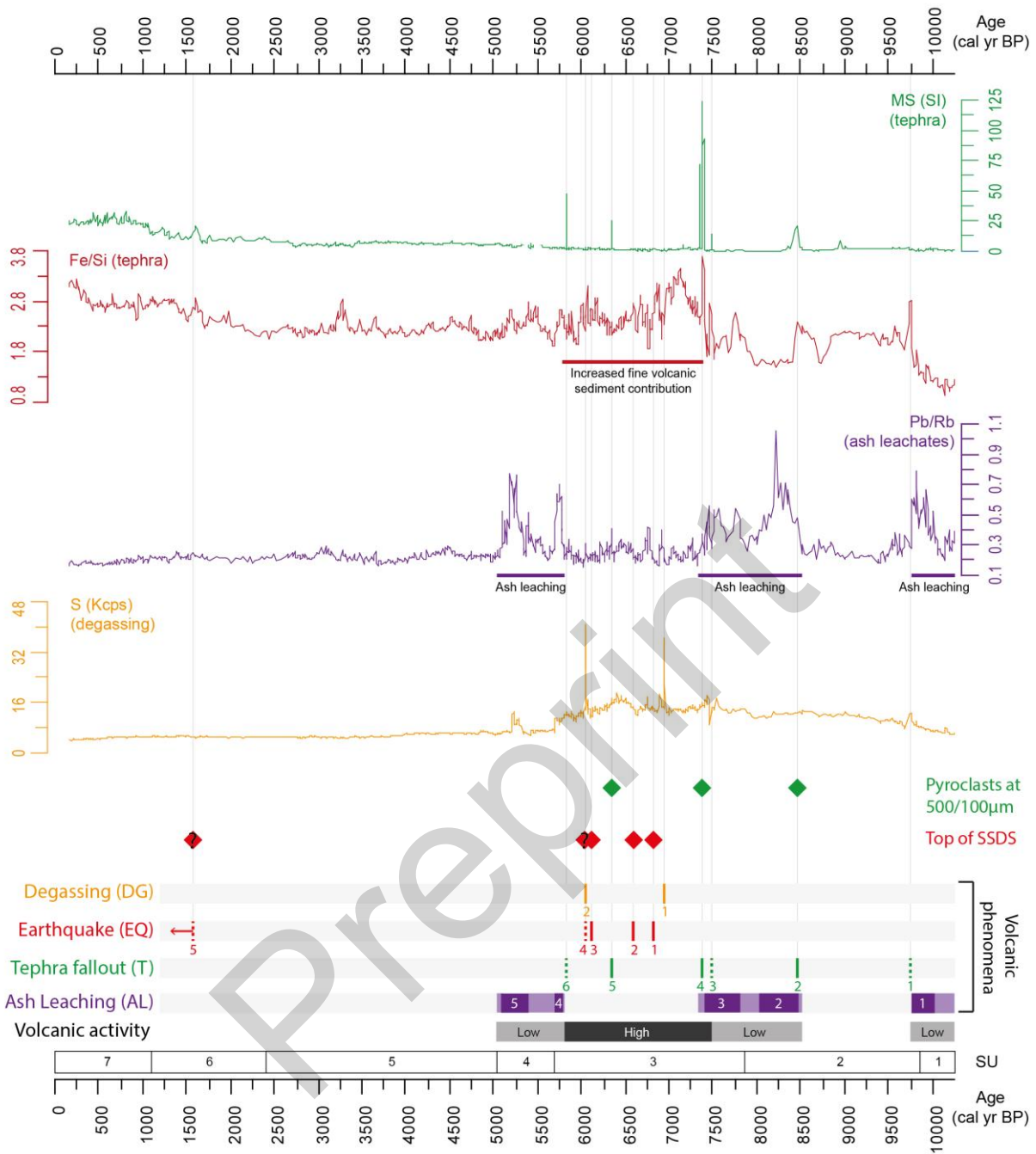
548 Three major phases of increased Pb/Rb signal can be identified in the MDSC sequence, and are
549 interpreted as gradual Pb inputs from ash leaching in the catchment (see results). The first phase
550 (AL1, 10,250–9750 cal yr BP approx.) occurs during the onset of wet conditions in the Sarliève
551 depression (contact between SU1B and SU2A): ash leachates from older tephra fallouts (probably
552 CF1 in the Lateglacial, not recorded in the MDSC, see introduction) probably reached the basin with

553 the first hydro-sedimentary inputs. The sudden interruption of this leaching by T1 at c. 514–515 cm
554 could be due to the modification of physico-chemical equilibriums in the soils of the catchment by
555 this new fallout, perhaps inhibiting leaching in favour of other processes. A second phase (8500–7400
556 cal yr BP approx.) is bracketed by tephtras T2 and T4, and can be subdivided into two episodes of
557 more marked ash leaching (AL2 and 3) separated by relatively lower Pb/Rb values. AL2 shows a
558 particularly strong leaching signal just after T2, suggesting that its Pb content could have been
559 massively leached and reached the basin in the centuries following the fallout. AL3 shows a
560 succession of smaller peaks, indicating renewed but less intense leachate inputs from the previous
561 fallout after a short period of reduced leaching around 7800–8000 cal yr BP. The end of AL3 coincides
562 with T3, and especially with T4, suggesting that these new fallouts could have interrupted leaching in
563 favour of other processes, such as in T1 (see above). The third phase of Pb enrichment in the
564 sequence (5800–5100 cal yr BP approx.) is also divided into two distinct events, AL4 and AL5. The
565 first one is a marked narrow peak (5800–5700 cal yr BP.) just following T6, indicating immediate
566 leaching of Pb from the fallout. AL5 is a larger peak (5400–5100 cal yr BP.) unassociated with any
567 tephra; it could represent a renewal of T6 leaching due to wetter conditions after the mid-Holocene
568 climatic shift (Steig, 1999; Fletcher et al., 2013; Zielhofer et al., 2019), or even an unknown fallout c.
569 5250 cal yr BP.

570 Five episodes of high seismic activity (earthquakes) were identified from SSDS layers (see results).
571 Earthquakes (EQ) 1 and 2 occurred circa 6800 and 6600 cal yr BP respectively. EQ3 and 4 were very
572 close in time, at around 6050–6100 cal yr BP. The sedimentary signature of EQ4 is uncertain, but the
573 event is remarkably coincident with a degassing event (see before). EQ5 affected the Sarliève Dark
574 Layer, but from the litho-stratigraphic description, it is unclear whether it occurred around 1600 cal
575 yr BP or a few centuries after, because the upper boundary of the disturbed layers cannot be
576 properly identified because of pedoturbation phenomena.

577 A clear phasing emerges from the chronological distribution of all these volcanic phenomena
578 recorded in the MDSC from the Early and Middle Holocene. Three phases of secondary impacts of
579 volcanism (gradual leaching of previous fallouts in the catchment) surround a high volcanic activity
580 phase between 7500 and 5800 cal yr BP, identified for the first time in the region. This phase,
581 corresponding roughly to SU3, includes four episodes of volcanic fallout (T3 to T6), and almost all the
582 detected seismic and degassing events. Its chronology is not out of place, as Mid-Holocene volcanic
583 activity is documented in the Chaîne des Puys and the neighboring Cézallier (Fourmont et al., 2006;
584 Boivin et al., 2017), and is deserving of dedicated investigations at a larger scale in the future.

Preprint



585

586 **Figure 9.** Sedimentological, chemical, and litho-stratigraphic indicators of volcanic phenomena in the MDSC
 587 sedimentary sequence. Elementary signals are in cps, ratios are dimensionless. Detected volcanic phenomena
 588 are numbered in chronological order. Less certain events are marked with "?", or dashed lines. Purple hue
 589 reflects the intensity of ash leaching from soils of the catchment. MS: magnetic susceptibility ($SI \cdot 10^{-5}$), SSDS:
 590 soft-sediment deformation structures.

591

592 We compared all these new findings with up-to-date regional volcanic chronology,
593 tephrostratigraphy, and palaeoseismology, to assess possible correlations. The proposed
594 chronological assemblage in Fig. 10 constitutes a first approach, and is subject to future refinements,
595 awaiting the forthcoming detailed physico-chemical analysis of the new tephra layers. Events
596 detected in the Early Holocene and at the beginning of the Middle Holocene (before 7500 cal yr BP,
597 AL1-3 and T1-2, see Fig. 10) are difficult to match with the volcanic chronology because of the
598 abundance of eruptions (most of them poorly dated) and the relatively low precision of the BADM in
599 lower parts of the core. After 7500 cal yr BP, the correlations are more certain because of less
600 volcanic eruptions and more accurate chronologies. T3, and especially T4, are probably related to the
601 tephra of the Pavin maar (Juvigné and Gilot, 1986; Boivin et al., 2011), and T5 is almost certainly the
602 G1/M1 tephra recently detected in the nearby Forez range (Jouannic et al., 2014).

603 Correlations between T6, AL4, and AL5, and the “Tephra de Sarliève” and the “Tephra de Beaunit”
604 (Fig. 10), are less straightforward, and interpretations are subject to caution. These two chemically
605 different tephras are very close in time and not well dated (Juvigné et al., 1986; Vernet, 2005;
606 Fourmont et al., 2006; Vernet et al., 2011). A first examination of the chronological structure of the
607 events suggests that T6 could be the “Tephra de Beaunit”, and AL4 the subsequent ash leaching
608 episode. In this case, the “Tephra de Sarliève” would not have been directly detected in the MDSC
609 core, but its leaching would correspond to AL5. However, the accepted date of c. 5400 cal yr BP for
610 the Tephra de Sarliève (Fig. 10, Fourmont et al., 2006) is in fact based on the PCE chronology, which
611 we consider to be under-aged by c. 400 years at this point (Fig. 8). Therefore, we believe the true age
612 of this tephra following the BADM is c. 5800 cal yr BP, i.e., almost the same as the “Beaunit Tephra”
613 and T6. This complex situation will only be disentangled by a detailed comparative analysis of the
614 involved tephra layers in the forthcoming years.

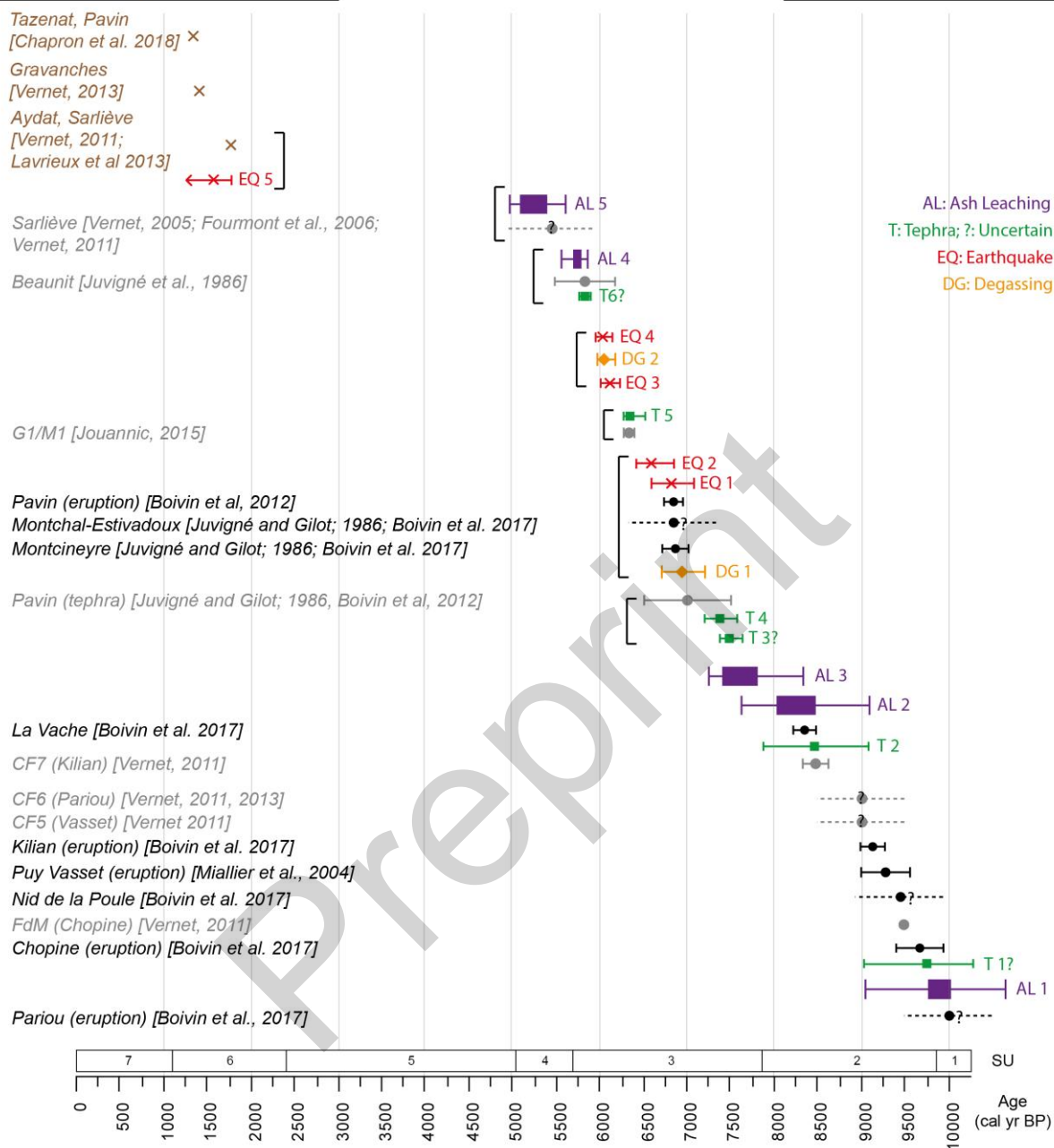
615 Two clusters of degassing events associated with earthquakes are also evident between 7000 and
616 6000 cal yr BP (Fig. 10), suggesting that the earthquakes were caused by volcanic rather than tectonic

617 activity. The first cluster (DG1 and EQ1–2, 7000–6500 cal yr BP approx.) seems quite clearly related
618 with three highly-explosive eruptions very close in time (Pavin, Montchal-Estivadoux, and
619 Montcineyre, see Juvigné and Gilot, 1986; Boivin et al., 2011, 2017). The association of the second
620 cluster (DG2 and EQ3–4, c. 6200–6000 cal yr BP) with volcanic activity related to the fallout of the
621 “Tephra de Beaunit” is unclear, especially considering the chronological uncertainty. Finally, a single
622 earthquake (EQ5) in historical times could be related to at least three earthquakes detected in
623 different wetlands and volcanic lakes in the surrounding region during the first centuries of our era
624 (Fig. 10, see Lavrieux et al., 2013; Vernet, 2013; Chapron et al., 2018), including one affecting the
625 Sarliève marsh, which seems the most plausible (Vernet et al., 2011).

Preprint

Local volcanic chronology;
Tephrochronology;
Palaeoseismology

Volcanic phenomena
recorded in MDSC core



626

627 **Figure 10.** Comparisons of volcanic phenomena recorded in the MDSC core with local volcanic chronology,
 628 tephrochronology, and palaeoseismology. References are given in brackets. Dates are plotted with their known
 629 age uncertainties (from literature or from BADM). When the latter are lacking, ages are plotted with a default
 630 uncertainty of ± 500 years (dashed lines). AL events are plotted as an interval, with the uncertainties of their
 631 extremes. Black brackets indicate possible clusters of associated phenomena/events.

632

633 4.3 Chronological review of the Holocene hydro-sedimentary history of the Sarliève basin

634

635 The new analytical data and the accurate chronological framework allow us to propose a renewed
636 interpretation of the Holocene hydro-sedimentary history of the basin, and to reassess the weight of
637 climatic, anthropogenic, and volcanic drivers (Fig. 11).

638

639 The distinctive characteristics of the base of the sequence (SU1, before 9800 cal yr BP, although the
640 BADM is imprecise here) suggest a highly mineral, authigenic, and very well-oxygenated carbonated
641 environment, rich in fine particles with some coarser inputs (see results and Fig. 11). These features
642 are highly congruent with a marly substratum reworked by colluvial processes, as proposed in
643 previous works (Fourmont, 2006; Fourmont et al., 2009), and probably dating to the cold phases of
644 the very Early Holocene (Preboreal) or even the Lateglacial, although no date supports this
645 chronology.

646

647 The overall palaeoenvironmental picture for SU2A and B (9800–7800 cal yr BP) is also broadly
648 consistent with previous works (Bréhéret et al., 2008; Fourmont et al., 2009; Macaire et al., 2010),
649 despite small chronological differences. The onset of aquatic conditions in the basin seems to occur
650 c. 9800 cal yr BP (base of SU2A), with higher values of Sr/Ca and F2 (Fig. 11) indicating an evaporitic
651 carbonated lake, likely endorheic, with formation of authigenic carbonates. The high values of Si, Al,
652 K, Fe, Rb, and Zn (see Fig. 7) in a general context of reduced detrital inputs suggest a small and
653 extremely mineral waterbody with a high dissolved load, consistent with the absence of *Ruppia*
654 *maritima*. This mineral enrichment could be due to dissolved products from Lateglacial volcanic
655 fallouts (Fourmont et al., 2006), but also to seepages from mineral springs, which are locally very
656 common in depressed areas controlled by faults such as the Sarliève basin (Ballut, 2000), and could
657 have represented a significant contribution to this first lake. Around 9100 cal yr BP, these conditions
658 change to those of a more permanent waterbody, indicating slightly wetter conditions than those of

659 previous periods, although still with evaporitic phases (SU2B, Fig. 11). The first apparition of *Ruppia*
660 *maritima*, fragments of ostracods (Fig. 6), and a much finer sedimentary matrix, suggest more
661 abundant and permanent saline waters (pre-evaporitic?) with some detrital inputs (presence of
662 sands). Authigenic carbonate formation in this playa-like salt lake seems to have been dominated by
663 high-Mg calcite or dolomite (see sedimentological data), as suggested by other authors (Bréhéret et
664 al., 2008; Fourmont et al., 2009).

665

666 The beginning of SU3 (c. 7800 cal yr BP) is characterized by the onset of irregular hydrological
667 conditions in the basin, as suggested by the apparition of the first bundles of laminae (Bréhéret et al.,
668 2008; Fourmont et al., 2009). Otherwise, carbonated sedimentation is markedly evaporitic and the
669 waterbody is brackish (presence of *Ruppia maritima*, Fig. 11). The period between 7400 and 6300 cal
670 yr BP approx. is characterized by a totally different sedimentary environment and highly changing
671 hydrological conditions, alternating between evaporitic and marshy phases (Sr/Ca, Fe/Mn,
672 abundance of laminae). The sediment accumulation rate increases, as does the D50, indicating more
673 abundant and higher energy detrital inputs dominated by silts (Fig. 6). Evaporitic phases are rather
674 characterized by deposition of authigenic carbonates in laminations (for details see Bréhéret et al.,
675 2008), whereas marshy phases feature siliceous sedimentation (Fig. 11), mainly detrital silts, but
676 certainly also some authigenic silicates such as quartz, feldspar, zeolites, and smectites (Fourmont,
677 2006; Fourmont et al., 2009). Between 6300 and 5700 cal yr BP, hydrological conditions remain
678 similar, but become gradually wetter and more stable with predominantly marshy conditions (few
679 laminations) and very short and weak evaporitic phases, probably due to wetter conditions during
680 the recent Atlantic period. The accumulation rate reaches extreme values (above 1 cm/year) by the
681 end of the phase. The particular sedimentological and geochemical features between 7400–5700 cal
682 yr BP are suggestive of a forcing of the hydro-sedimentary system, which caused massive and quick
683 inputs of silty siliceous sediments (or dissolved siliceous load) into the basin.

684

685 These findings are in general agreement with those of previous research works, which proposed that
686 the development of agricultural activities during the first phases of neolithization c. 7400 cal yr BP
687 could have caused significant soil erosion and exceptionally quick accumulation rates in the Sarliève
688 marsh from the beginning of SU3.

689 However, these interpretations are undermined by a number of significant flaws: first, an
690 anthropogenic cause for this dramatically increased sediment supply to the basin is not clearly
691 established in sediment yield studies (Macaire et al., 2010). Second, only very weak evidence of Early
692 Neolithic occupations (two sherds dating to the end of the Early Neolithic, i.e., before c. 6500 yr BP)
693 have been detected by archaeological prospection in the catchment (Trément et al., 2007).
694 Moreover, agricultural developments during such an early period were rather limited (Delpuech,
695 1987), and increases in soil erosion were very local (Mayoral, 2018; Mayoral et al., 2020a). In
696 summary, these considerations suggest that the local small Early Neolithic communities are unlikely
697 to have caused such a strong sudden catchment-scale (c. 30 km²) impact on soil erosion at Sarliève
698 since 7400 cal yr BP.

699
700 The results of the work described in this study suggest an alternative and more complex scenario for
701 the deposition of SU3 between 7400 and 5700 cal yr BP. The unit has very specific features that are
702 not repeated in any of the other detrital phases during later periods. The markedly siliceous and
703 volcanic nature of the fine sediment (low F2, high Fe/Si, see Figs. 9 and 11), contrasting with the
704 carbonated nature of the catchment and with an absence of granitoids or sandstones, points to a
705 source in siliceous volcanic materials. Geochemical analysis in the catchment (Fourmont, 2006;
706 Fourmont et al., 2009) showed that some samples of SU3 had a composition close to that of the
707 volcanic rocks of the catchment, especially the tephras. Additionally, sedimentological data (see
708 results) indicate either a very well-sorted and homogeneous silty source material instead of generic
709 soil erosion, or a silt-focused transport process (such as aeolian transport), or both. Finally, the
710 extremely high accumulation rate suggests a temporarily very abundant and available sedimentary

711 source. Finally, the chronology of SU3 coincides remarkably well with the detected cluster of intense
712 volcanic activity between 7400 and 5800 cal yr BP (see above), which includes four potential tephra
713 layers (T3 to T6, Fig. 10).

714

715 Therefore, SU3 can be only interpreted as the result of local to micro-regional production of massive
716 quantities of very fine volcanic ash (silt-sized, extremely well sorted and rich in Si, Al or Fe) by
717 sudden and intense volcanic activity from c. 7400 until 5800 cal yr BP. Unconsolidated volcanic ash
718 and dust deposits (from one or several rhyolitic or trachyandesitic eruptions) would have been
719 completely removed from the catchment, mainly by aeolian deflation, but secondarily by runoff and
720 dissolution, and would be finally trapped in the Sarliève basin, which was endorheic by this time
721 (Fourmont et al., 2009). The deposits accumulated quickly, forming a thick layer of well-sorted fine
722 siliceous material mixed with minor amounts of detrital materials from soil erosion and authigenic
723 carbonates. The formation of authigenic silicates occurred probably from the dissolution of the ashes
724 in the brackish water, or from high inputs of dissolved Si from ashes in the catchment, as suggested
725 by Fourmont (Fourmont, 2006; Fourmont et al., 2006; Fourmont et al., 2009). All these processes, in
726 combination with the gradually wetter conditions detected after 6300 cal yr BP, are the likely causes
727 of the exceptionally high accumulation rates of well-sorted silty silicates in the basin between 7400
728 and 5600 cal yr BP (Fig. 5 & 11), with a paroxysm at c. 5800–5700 cal yr BP (peak of SAR coincident
729 with the T6 fallout). This volcanic forcing of the hydro-sedimentary system during the Middle
730 Holocene at Sarliève questions the classical morpho-sedimentary narrative in the Limagne lowlands,
731 i.e., that of increased erosion and floodplain aggradation due to volcanic activity in the Lateglacial
732 and Early Holocene, followed by rather low-energy dynamics in the Mid-Holocene (Ballut, 2000;
733 Vernet and Raynal, 2002; Raynal et al., 2003). The comprehensive understanding of interactions
734 between volcanos, climate, and humans during this period is a complex challenge that is beyond the
735 scope of this work and will require further multidisciplinary studies.

736 These dynamics changed abruptly from the beginning of SU4; during the phase between 5700 and
737 5000 cal yr BP, the hydrological conditions were permanently marshy and brackish with few weak
738 evaporitic phases (presence of *Ruppia maritima* but absence of laminations). The sedimentary
739 accumulation rate falls quickly, as does the D50, indicating much less and weaker sedimentary inputs,
740 although the siliceous fraction is still dominant at the beginning of the phase. The main reason for
741 this marked sedimentary slowdown is probably the end of the intensive volcanic activity and volcanic
742 ash inputs after 5800 cal yr BP (Fig. 9). However, less important archaeological occupations and
743 reduced anthropogenic pressure on soils during the beginning of the Late Neolithic (Trément et al.,
744 2007; Macaire et al., 2010) could also have contributed. From a grain-size and textural perspective,
745 this phase is very similar to SU2, suggesting a relative recovery of previous sedimentary processes
746 after the forcing represented by SU3 (Fig. 6), although under clearly wetter conditions since
747 approximately 6300 cal yr BP. This phase was nevertheless transitory, as a new detrital signal
748 emerged and grew gradually from c. 5500 cal yr BP (Fig. 11).

749
750 This detrital signal increases steadily during the next phase (SU5, 5000–2500 cal yr BP approx.), while
751 the water level continued to rise. The sedimentary environment of SU5 was probably that of a
752 permanent freshwater carbonated lake (absence of *Ruppia maritima* and laminations, lacustrine clay
753 facies with an abundance of ostracods, *Characeae* gyrogonites, and *Daphnia ephippia*), consistent
754 with the interpretations proposed in previous work (Bréhéret et al., 2008; Fourmont et al., 2009 i.a.).
755 A rise of the outlet level (perhaps due to a mudflow, see Fourmont, 2006) combined with wetter
756 conditions after the Mid-Holocene hydroclimatic shift would have led to an increase in the water
757 level and the connection of both sub-basins.

758
759 During the first phase (5000–3600 cal yr BP approx.) of the lake at Sarliève, the accretion rate
760 remains very low, but the relative detrital influx becomes gradually stronger, reaching a peak at c.
761 3700–3600 cal yr BP. The D50 signal, despite its relatively low resolution, indicates an increase in the

762 energy of the detrital inputs, suggesting more concentrated runoff. Forcing of soil erosion by Late
763 Neolithic societies seems plausible here from 5000, or perhaps 5500 cal yr BP, in agreement with the
764 marked increase in the intensity of erosion and in the sedimentary yield that previous works
765 interpreted as anthropogenic at Sarliève (Macaire et al., 2010), but also with other lacustrine records
766 in the Massif Central with roughly similar chronologies (e.g. Martin et al., 2019). Remarkably, this is
767 rather a phase of site abandonment and reduced erosion in the neighboring volcanic plateaus of the
768 Limagne (Mayoral et al., 2020a), suggesting that settlements could have moved to the lowlands.
769 Between 3600 and 2500 cal yr BP (following the BADM) the picture becomes more complex: just
770 after 3600 cal yr BP the detrital influx and the D50 fall abruptly, indicating less erosion in the
771 catchment. This situation is maintained until approximately 3000 cal yr BP, when both indicators rise
772 again and maintain high values until c. 2500 cal yr BP. This phase of reduced erosion and detrital
773 inputs coincides with the Middle Bronze age and the first part of the Late Bronze age, two cultural
774 periods poorly known at local and regional scales because of a marked lack of remains, but
775 characterized by abandonment of previous habitats and a reduced number of settlements compared
776 with the Early Bronze age and the end of the Late Bronze age (Trément et al., 2007; Couderc, 2019).
777 It is therefore likely that less human impacts during this phase were the reason for the significant
778 reduction in soil erosion and detrital inputs into the basin, followed by a recovery by the end of the
779 Late Bronze age, as noted elsewhere in Limagne (e.g. Mayoral et al., 2020b).

780 Several short-lived lacustrine low-stands have been detected in SU5 from stratigraphy and
781 geochemical proxies (Fig. 11), most of them concentrated in the Middle and Late Bronze age. The
782 water level in the carbonated lake was lower at c. 4750–4600, 3750–3600, 3350–3200, and 2950–
783 2800 cal yr BP, indicating comparatively dryer periods. All of these are synchronous with well-
784 documented phases of low levels in western alpine lakes and dryer pedogenic phases in the Rhône
785 valley (Magny, 2004; Berger et al., 2007; Magny et al., 2007), pointing clearly to climatic control. In
786 general, these dryer phases are associated with favourable periods for expansion of human activities
787 in northern alpine Europe (Tinner et al., 2003). However, at Sarliève, a positive or negative

788 correlation with anthropogenic impacts in the catchment is not evident, suggesting that the local
789 influence of these otherwise small climatic oscillations on Late Neolithic and Bronze Age societies
790 was limited.

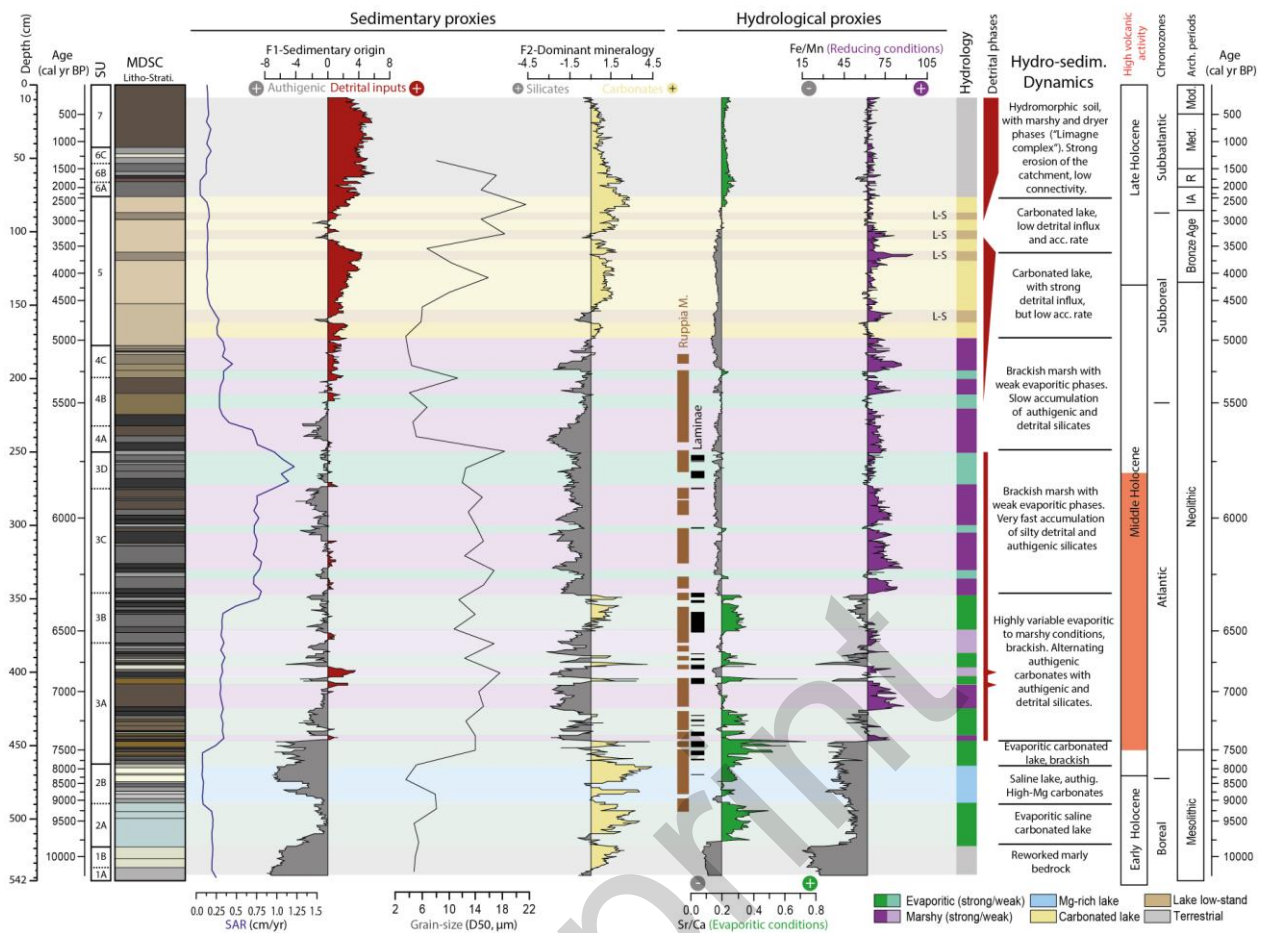
791 The carbonated lake represented by SU5 disappears abruptly and leaves in place SU6 at a depth of 76
792 cm. This unit (and also the current soil SU7) is in general terms a relatively dry hydromorphic soil,
793 with some phases of carbonated marsh. It is marked by a strong detrital influx due to the erosion of
794 the catchment, but the low accretion rate and the decreased D50 also suggest reduced hydro-
795 sedimentary connectivity, nowadays maintained by a dense network of drainage ditches (Fig. 1C).
796 The sharp transition between SU5 and SU6A, interpreted as a lake drainage phase (as the core is
797 situated in its deepest part), is dated in the BADM to c. 2400 ± 330 cal yr BP. However, this date can
798 be refined using radiocarbon 3 and 6 (2535 ± 170 and 2615 ± 124 cal yr BP respectively, see Table 1),
799 which are also considered in the dating of this event (see results), and suggest that the drainage
800 occurred between 2500 and 2600 cal yr BP approx. Date number 2 (2640 ± 118 cal yr BP) at 79 cm (3
801 cm below the top of SU5) also supports this chronological interpretation, as the accretion rate in this
802 section of the core is 0.125 cm/year (i.e., 8 years/cm). This precocious date for the drainage of the
803 lake is earlier than the chronology proposed by previous works (c. 2250 cal yr BP, Trément et al.,
804 2007; Macaire et al., 2010). A very similar date (c. 2600 cal yr BP) was recently proposed for the
805 drainage of la Narse de la Sauvetat, a similar although smaller wetland 8 km south of the Sarliève
806 marsh (Mayoral et al., 2018; Mayoral et al., 2020b), revealing a pattern of wetland drainage in
807 Limagne at the beginning of the second part of the first Iron Age. This chronology presumes that the
808 Hallstatt societies possessed significant hydraulic capacity and were able to drain and settle former
809 wetlands, as already detected in other French regions (Milcent and Mennessier-Jouannet, 2007;
810 Bernigaud et al., 2014; Riquier et al., 2015).

811

812 This drainage led to the development of a hydromorphic soil (SU6A, see Fig. 2) characterized by a
813 reduction in detrital inputs, a less-carbonated mineralogy, and a shift towards a slightly evaporitic

814 regime (F1, F2, Sr/Ca in Fig. 11). The presence of this soil between the drainage of c. 2550 cal yr BP
815 and the development of marshy conditions in Roman times (see below) fills a supposed hiatus of
816 several centuries (Fourmont et al., 2009; Macaire et al., 2010), opening room for the study of the
817 Iron Age in the sequence, which is a major period of anthropogenic impact in Limagne (Trément et
818 al., 2007; Mayoral, 2018). The sudden onset of marshy conditions in the IIIrd c. AD (c. 1716 cal yr BP,
819 date 1, 65 cm) is reflected by the level of dark sediment known as the “Sarliève Dark Layer” (SU6B,
820 see Vernet, 2005; Vernet et al., 2011). This layer reflects a palustrine environment with reduced
821 detrital inputs, but appears in detail much more complex than depicted in previous works: four
822 different sub-layers indicate changing hydro-sedimentary conditions (F1, F2, and Fe/Mn in Fig. 11) in
823 the Sarliève basin from the IIIrd c. AD and during the Late Antiquity, similar to other Limagne
824 wetlands. The exact nature and causes of these quick changes remain unclear, but they are more
825 likely to be due to major modifications in landscape management than to climatic degradation
826 (Mayoral et al., 2020b), although this should be confirmed by further studies. The hydrosedimentary
827 dynamics after the Late Antiquity cannot be inferred from the sequence because of pedo- and
828 agroturbation; however, the presence of a marsh or lake in the basin during the Middle Ages is
829 known from historical sources (Trément et al., 2007). This medieval lake was finally drained in the
830 XVIIth century, after which the Sarliève marsh became a permanently cultivated plain.

831



832

833 **Figure 11.** Multi-proxy reconstruction of Holocene hydro-sedimentary dynamics in the Sarliève marsh.

834 Baselines for Fe/Mn and Sr/Ca correspond to the mean values. Chronozones and archaeological periods are

835 from Maccare et al., 2010. IA: Iron Age, R: Roman, Med.: Medieval, Mod.: Modern, SAR: sediment accumulation

836 rate, L-S: lacustrine low-stand

837

838

839

840

841

842

843 5. CONCLUSIONS

844

845 Sedimentological and geochemical analyses were performed on a new sedimentary core from the
846 Sarliève marsh, and are interpreted within a radiocarbon-based Bayesian age-depth model
847 significantly more accurate than any previous models or estimations, which were in some cases
848 extremely divergent. On this basis we proposed a thorough review and reinterpretation of the
849 Holocene volcanic events and hydro-sedimentary history recorded in the sedimentary sequence.

850 We detected an array of new volcanic phenomena recorded in the Sarliève marsh: six (crypto)tephra
851 fallouts were identified, five of them previously unknown in the Sarliève sedimentary sequence (c.
852 9750, 8500, 7500, 7400, 6300, and 5800 cal yr BP). Five unknown earthquakes (c. 6800, 6600, 6050,
853 6100, and 1600 cal yr BP) and two degassing events (c. 6950 and 6050 cal yr BP) were also detected
854 for the first time. This concentration of fallouts, earthquakes, and degassing episodes depict a
855 hitherto unsuspected phase of intense volcanic activity in the Limagne during the Middle Holocene,
856 between 7500 and 5800 cal yr BP. Three phases of residual volcanic impacts characterized by slow
857 leaching of previous ash deposits were detected between 10,250–9750, 8500–7400, and 5800–5100
858 cal yr BP. Although requiring further detailed studies and cross-validation, several of these findings
859 can be matched with known events, enriching the regional volcanic chronology, tephrochronology,
860 and seismochronology.

861 The hydro-sedimentary history of the Sarliève marsh was also substantially reviewed and
862 reinterpreted thanks to the new chronology and high-resolution analysis, with integration of the new
863 volcanic data. Consistent with previous works, our data suggest that between c. 9800 and 7800 cal yr
864 BP, the basin was endorheic and occupied by a small highly-mineral and saline waterbody with a
865 marked evaporitic regime. The basin evolved to a brackish marsh between 7800 and 7400 cal yr BP,
866 probably because of a wetter climate, but its hydrology became irregular with several evaporitic
867 episodes. From 7400 to 5700 cal yr BP, hydrological conditions became gradually wetter (especially

868 from 6300 cal yr BP onwards) and the basin received massive inputs of extremely well-sorted
869 siliceous silts. These sediments have characteristics compatible with reworked fine volcanic ash,
870 probably discharged by the detected increase in volcanic activity during this period, and accumulated
871 in the marsh by wind or runoff. Our results suggest that the massive catchment-scale sedimentary
872 forcing during this phase was mainly volcanic, and that the role of climate and Neolithic societies
873 proposed in previous works was minor. These results, which should be confirmed by further works,
874 question the Holocene morpho-sedimentary narrative in Limagne.

875 From 5700 cal yr BP and immediately after the end of the phase of high volcanic activity, the
876 sediment accumulation rate decays and the basin seems to return to something of a pre-forcing
877 state, although with significantly wetter conditions. However, this phase is relatively short-lived, as
878 from 5000 cal yr BP major changes occur: a rise in water level due to wetter conditions after the Mid-
879 Holocene climatic shift transformed the marsh into a carbonated freshwater lake, and an
880 anthropogenic detrital influx developed from 5500 cal yr BP. This signal of increased erosion probably
881 due to the impacts of Late Neolithic societies on soils is consistent with previous works, and grows
882 more clearly after 5000 cal yr BP. However, our results suggest a hitherto undetected lull in erosion
883 and detrital influx into the basin between 3600 and 3000 cal yr BP, probably related to a regionally
884 well-documented abandonment of habitat and decrease of activity during the Middle and the
885 beginning of the Late Bronze age, followed by a recovery at the end of the period. A series of low-
886 stands of the lake indicating dryer periods occurred during this phase (c. 4750–4600, 3750–3600,
887 3350–3200, and 2950–2800 cal yr BP). Their synchrony with similar events in the Rhône valley and
888 the western alpine lakes point to climatic control. However, these small variations in precipitation
889 are not clearly connected with detrital influx from the catchment and anthropogenic erosion,
890 suggesting here a rather reduced influence of climate on protohistoric societies.

891 The results suggest that this lake could have been drained c. 2550 cal yr BP, i.e., several centuries
892 earlier than previously accounted. This allows us to hypothesize that Early Iron age societies could

893 have had a significant hydraulic capacity, and pulls back the date for this major threshold in
894 anthropogenic impacts on wetlands. The development of a hydromorphic soil after this first major
895 drainage phase shows that there is no hiatus in the sedimentary sequence between the late Iron Age
896 and the IIIrd c. AD (Roman times), opening new possibilities for palaeoenvironmental studies of this
897 period at Sarliève. Finally the Sarliève Dark Layer, corresponding to the development of a marsh from
898 c. 1716 cal yr BP and during the Late Antiquity, appears more complex than previously thought. Its
899 interpretation as the result of rapid hydro-sedimentary changes due to land-use modifications,
900 similar to other Limagne wetlands, demands dedicated studies.

901 Ultimately, this work outlines the complexity and non-linearity of the interactions between hydro-
902 sedimentary systems, climate, volcanos, and Protohistoric societies, and highlights the utility of high-
903 resolution multiproxy analysis of sedimentary archives and the crucial importance of reliable age-
904 depth models to disentangle the causality. In Limagne, where high quality and well-dated Holocene
905 palaeoenvironmental records are particularly rare, the results of this study should form a
906 cornerstone for forthcoming detailed studies.

907 6. ACKNOWLEDGEMENTS

908 This work was funded by the Conseil Départemental du Puy-de-Dôme (F.), within the program
909 “L’Oppidum de Gergovie: contexte Géomorphologique, Paléoenvironnemental et Géoarchéologique”
910 (Dir. Y. Miras & E. Defive). The authors want to acknowledge the landowner, M. Vivier, who allowed
911 access to his fields. We are also grateful to a number of people who contributed to this work with
912 their support in the field, laboratory assistance, administrative work, or valuable scientific
913 discussions: Aude Beauger, Elisabeth Allain, Ana Ejarque, Arthur Ancrenaz, Laura Benedito, Yann
914 Deberge, Manon Cabanis, Franck Vautier, Bertrand Dousteysier, Florian Couderc, Delphine Latour,
915 Anne-Lise Develle, Marion Dacko, Bruno Depreux, Hector Orengo and Marc Récoché. Finally, we
916 express sincere thanks to the anonymous reviewers for their remarks and critical reading of the
917 manuscript.

SU	Depth (cm.)	Description (color, texture, inclusions, sed. structures, pedofeatures)	
7	0–42.5	Topsoil. Grey silty clays, brownish at the top, sparse sands and granules, pedogenic aggregation (blocky subangular to granular)	
6C	42.5–53.5	Grey silty clays, including abundant beige mottles, some dark mottles, sparse sands and granules, pedogenic aggregation (blocky subangular to granular)	
6	6B	53.5–66	Complex level including several layers of dark brown, dark-grey to black, and grey silty clays, small beige and dark mottles and sparse sands and granules (“Sarliève Dark Layer”). Pedogenic aggregation (blocky subangular to granular) disturbed by post-depositional deformations (mutual inclusions of different layers)
6A	66–76	Dark-grey silty clays with abundant small light and dark mottles, sparse sands and pedogenic aggregation (blocky subangular, top)	
5	76–177.5	Homogeneous light-grey to beige clays (with some sections slightly darker), sparse silty and sandy particles, some small dark dots, and traces of incipient pedogenesis from upper levels (incipient aggregation above 100 cm –blocky subangular to angular– and small rootlets in all the unit).	
4C	177.5–199.5	Succession of layers of dark-grey to light-grey and brownish-grey clays, rare and sparse <i>Ruppia maritima</i> seeds (base), beige and dark small mottles in layers. Few small reddish oxidation mottles at the base. One isolated dark layer at the top of the unit.	
4	4B	199.5–232	Brownish grey clays, with <i>Ruppia maritima</i> seeds, sometimes with small dark mottles. Two centimetric intrusions of brown clays, with pedogenic aggregation (subangular to granular), rich in big vegetal debris, and sparse sands and granules.
4A	232–249	Grey to dark-grey clays, with some <i>Ruppia maritima</i> seeds.	
3D	249–274.5	Light-grey and grey clays, with some <i>Ruppia maritima</i> seeds sometimes bedded. Very abundant and very fine (infra-mm) dark, brown, and beige, sometimes reddish <i>laminae</i> , diffuse to very well marked, in bundles or isolated.	
3C	274.5–346	Grey, dark-grey, and brownish grey clay layers, sometimes with abundant <i>Ruppia maritima</i> seeds, and very rare <i>laminae</i> . Lower half disturbed by SSDS (micro-faulting, intrusion of liquefied material from lower levels).	
3	3B	346–380	Grey to dark-grey clays, sometimes with abundant <i>Ruppia maritima</i> seeds. Very abundant and very fine brown, greenish, dark, and beige <i>laminae</i> , isolated or in bundles. SSDS at the top (cusp structure, load cast, micro-faulting).
3A	380–462.5	Layers of dark-grey, grey, brown, beige, and greenish clay, with abundant <i>Ruppia maritima</i> seeds. Abundant and fine (infra-mm) but also thick (millimetric) beige, brown, dark, and greenish <i>laminae</i> (or bedded <i>maculae</i>) more or less defined and sometimes arranged in bundles or in irregular beige-brown-grey sequences with <i>Ruppia</i> seeds. Central and upper part disturbed by SSDS (mixed layer, intruded material, mushroom-like structure, micro-faulting).	
2	2B	462.5–489	Diffuse light-grey to beige clay layers with some <i>Ruppia maritima</i> seeds, one brown diffuse lamination.
2A	489–519	Quasi homogeneous, very diffuse layers of beige to bluish-grey clays with dark and beige small mottles	
1	1B	519–533	Beige silty clays with some fine sand, some darker mottles (top)
1A	533–542	Greyish-beige silty clays with some fine sands, several beige and grey mottles	

920 **Table A.1.** Synthetic litho-stratigraphic description of the MDSC core. SSDS: soft-sediment deformation structures.

928 **8. REFERENCES**

- 929 Armit, I., Swindles, G. T., Becker, K., Plunkett, G., & Blaauw, M., {2014}. Rapid climate change did not
 930 cause population collapse at the end of the European Bronze Age. *Proceedings of the National*
 931 *Academy of Sciences*, 111, 17045–17049.
- 932 Ayris, P. M., & Delmelle, P., {2012}. The immediate environmental effects of tephra emission. *Bulletin*
 933 *of Volcanology*, 74, 1905–1936.
- 934 Bajard, M., Sabatier, P., David, F., Develle, A.-L., Reyss, J.-L., Fanget, B., Malet, E., Arnaud, D.,
 935 Augustin, L., Crouzet, C., Poulenard, J., & Arnaud, F., {2015}. Erosion record in Lake La Thuile
 936 sediments (Prealps, France): Evidence of montane landscape dynamics throughout the
 937 Holocene. *The Holocene*, 26, 350–364.
- 938 Baldini, J. U. L., Brown, R. J., & Mawdsley, N., {2018}. Evaluating the link between the sulfur-rich
 939 Laacher See volcanic eruption and the Younger Dryas climate anomaly. *Climate of the Past*, 14,
 940 969–990.
- 941 Ballut, C., {2000}. Evolution environnementale de la Limagne de Clermont-Ferrand au cours de la
 942 seconde moitié de l’holocène (Massif central français). Université de Limoges.
- 943 Barathon, J., & Valleix, J., {1993}. Les processus érosifs en Limagne clermontoise : aspects historique
 944 et contemporain d’ un phénomène social (Erosion processes in Limagne around Clermont :
 945 historical and contemporary aspects of a social phenomenon). *Bulletin de l’Association de*
 946 *géographes français*, 5, 471–488.
- 947 Beck, C., {2009}. Late Quaternary lacustrine paleo-seismic archives in north-western Alps: Examples
 948 of earthquake-origin assessment of sedimentary disturbances. *Earth-Science Reviews*, 96, 327–
 949 344.
- 950 Berger, J-F., Brochier, J. L., Vital, J., Delhon, C., & Thiébault, S., {2007}. Nouveau regard sur La
 951 dynamique des paysages et l’occupation humaine à L’Âge du Bronze en moyenne vallée du
 952 Rhône. In H. Richard, C. Mordant, & M. Magny (Eds.), *Environnements et cultures à l’Age du*
 953 *bronze en Europe occidentale* (p. 399). Paris: Editions du CTHS.
- 954 Berger, J-F., Carozza, J.-M., Carozza, L., Castanet, C., Cubizolle, H., Deschodt, L., Franc, O., Ghilardi,
 955 M., Lespez, L., Vannièrè, B., Salvador, P. G., Argant, J., Brochier, J. É., & Germaine, M.-A., {2018}.
 956 Climat et environnements : les étapes de la première anthropisation de l’espace (6000-2000
 957 BCE) en France. In J. Guilaine & D. Garcia (Eds.), *La protohistoire de la France* (p. 540). Hermann.
- 958 Bernigaud, N., Berger, J.-F., Bouby, L., Delhon, C., & Latour-Argant, C., {2014}. Ancient canals in the
 959 valley of Bourgoin-La Verpillière (France, Isère): morphological and geoarchaeological studies of
 960 irrigation systems from the Iron Age to the Early Middle Ages (8th century ~~bc~~BC–6th century
 961 ~~ad~~AD). *Water History*, 6, 73–93.
- 962 Blaauw, M., {2012}. Out of tune: The dangers of aligning proxy archives. *Quaternary Science Reviews*,
 963 36, 38–49.
- 964 Blaauw, M., & Christen, J. A., {2011}. Flexible paleoclimate age-depth models using an autoregressive
 965 gamma process. *Bayesian Analysis*, 6, 457–474.
- 966 Blott, S. J., & Pye, K., {2001}. Gradistat: A Grain Size Distribution and Statistics Package for the
 967 Analysis of Unconsolidated Sediments. *Earth Surface Processes and Landforms*, 26, 1237–1248.

- 968 Boivin, P., Besson, J.-C., Briot, D., Gourgaud, A., Labazuy, P., Langlois, E., De Larouzière, F.-D., Livet,
969 M., Médard, E., Mergoil, J., Merciecca, C., Miallier, D., Morel, J.-M., Thouret, J.-C., & Vernet, G.,
970 {2017}. *Volcanologie de la Chaîne des Puys* (6e Edition.). Château de Montlosier, 63970 Aydat:
971 Parc Naturel Régional des Volcans D’Auvergne.
- 972 Boivin, P., Besson, J.-C., Ferry, P., Gourgaud, A., Miallier, D., Thouret, J.-C., & Vernet, G., {2011}. Le
973 point sur l’éruption du lac Pavin il y a 7000 ans. *Revue des Sciences Naturelles d’Auvergne*, 74–
974 75, 45–55.
- 975 Bouiller, R., {1979}. Minute de la carte Géologique de la France à 1:50000, feuille 717 (Veyre-
976 Monton). BRGM.
- 977 Bourdier, J. L., Boivin, P., Gourgaud, A., Camus, G., Vincent, P. M., & Lenat, J. F., {1994}. Le
978 volcanisme. *Manuels et méthodes - Bureau de recherches géologiques et minières*. BRGM
979 éditions.
- 980 Bréhéret, J.-G., Macaire, J.-J., Fleury, A., Fourmont, A., & Soulié-Märsche, I., {2003}. Indices de
981 confinement dans les dépôts lacustres holocènes de Sarliève (Limagne, France). *Comptes
982 Rendus Geoscience*, 335, 479–485.
- 983 Bréhéret, J. G., Fourmont, A., Macaire, J. J., & Négrel, P., {2008}. Microbially mediated carbonates in
984 the Holocene deposits from Sarliève, a small ancient lake of the French Massif Central, testify to
985 the evolution of a restricted environment. *Sedimentology*, 55, 557–578.
- 986 BRGM, {1973}. *Carte Geologique 1/50.000 n°693 (Clermont-Ferrand)*. (BRGM, Ed.), Orléans: BRGM.
- 987 Brown, T. aA., Nelson, D. E., Mathewes, R. W., Vogel, J. S., & Southon, J. R., {1989}. Radiocarbon
988 dating of pollen by accelerator mass spectrometry. *Quaternary Research*, 32, 205–212.
- 989 Carozza, L., Berger, J.-F., Burens, A., & Marcigny, C., {2015}. Society and environment in Southern
990 France from the 3rd millenium BC to the beginning of the 2nd millenium BC a tipping point? In
991 2200 BC – Ein Klimasturz als Ursache für den Zerfall der Alten Welt ? 2200 BC – A climatic
992 breakdown as a cause for the collapse of the old world ? (pp. 833–844).
- 993 Cas, R. A. F., & Wright, J. V., {1987}. *Volcanic Successions. Modern and Ancient*. London: Springer
994 Netherlands.
- 995 Chapron, E., Chassiot, L., Foucher, A., & Lavrieux, M., {2018}. An up-to-date Holocene catalog of
996 sedimentary events recorded in volcanic lakes from the French Massif Central. In *ISC 2018 20th
997 International sedimentological Congress*.
- 998 Couderc, F., {2019}. La basse Auvergne (Puy-de-Dôme, sud Allier) : un espace privilégié pour l’étude
999 des territoires et des paysages de l’âge du Bronze. In *Colloque international anniversaire de l’
1000 APRAB* (pp. 94–97). Bayeux: APRAB.
- 1001 Cuyen, S., Francus, P., & Lamoureux, S., {2011}. Mid to Late Holocene hydroclimatic and geochemical
1002 records from the varved sediments of East Lake, Cape Bounty, Canadian High Arctic. *Quaternary
1003 Science Reviews*, 30, 2651–2665.
- 1004 Dearing, John. A., {1999}. Using the Bartington MS2 System. *Environmental Magnetic Susceptibility*,
1005 52.
- 1006 Delpuech, A., {1987}. *Deux millions d’années en Auvergne: archéologie et autoroute A 71*. Marsat:
1007 Direction des antiquités d’Auvergne; SAPRR.

- 1008 Dunbar, N. W., Iverson, N. A., Van Eaton, A. R., Sigl, M., Alloway, B. V., Kurbatov, A. V., Mastin, L. G.,
1009 McConnell, J. R., & Wilson, C. J. N., (2017). New Zealand supereruption provides time marker for
1010 the Last Glacial Maximum in Antarctica. *Scientific Reports*, 7, 3–10.
- 1011 Fisher, R., (1963). Bubble-wall texture and its significance. *Journal of Sedimentary Research*, 33, 224–
1012 227.
- 1013 Fisher, R. V., & Schmincke, H.-U., (1984). *Pyroclastic Rocks*. Berlin Heidelberg New York Tokyo:
1014 Springer-Verlag.
- 1015 Fletcher, W. J., Debret, M., & Sanchez-Goñi, M.-F., (2013). Mid-Holocene emergence of a low-
1016 frequency millennial oscillation in western Mediterranean climate: Implications for past
1017 dynamics of the North Atlantic atmosphere westerlies. *The Holocene* 23, 153-166.
- 1018 Fletcher, W. J., Zielhofer, C., Mischke, S., Bryant, C., Xu, X., & Fink, D., (2017). AMS radiocarbon dating
1019 of pollen concentrates in a karstic lake system. *Quaternary Geochronology*, 39, 112–123.
- 1020 Fourmont, A., (2006). Quantification de l'érosion et de la sédimentation dans le bassin de Sarliève
1021 (Massif Central, France) au tardiglaciaire et à l'Holocène : Impact des facteurs naturels et
1022 anthropiques. Université François Rabelais-Tours.
- 1023 Fourmont, A., Macaire, J.-J., Bréhéret, J.-G., Argant, J., Prat, B., & Vernet, G., (2006). Tephras in
1024 lacustrine sediments of the Sarliève marsh (French Massif Central): age and preservation.
1025 *Comptes Rendus Geoscience*, 338, 1141–1149.
- 1026 Fourmont, A., Macaire, J. J., & Bréhéret, J. G., (2009). Contrasted Late Glacial and Holocene hydrology
1027 of Sarliève paleolake (France) from sediment geometry and detrital versus biochemical
1028 composition. *Journal of Paleolimnology*, 41, 471–490.
- 1029 Fournier, J., Bonnot-Courtois, C., Paris, R., Voltaire, O., & Le Vot, M., (2012). *Analyses
1030 Granulométriques - Principes et Méthodes*. Dinard: CNRS.
- 1031 Gachon, L., (1963). Contribution à l'étude du Quaternaire récent de la Grande Limagne marno-
1032 calcaire : morphogénèse et pédogénèse. Institut National Agronomique.
- 1033 Grimm, E. C., Maher, L. J., & Nelson, D. M., (2009). The magnitude of error in conventional bulk-
1034 sediment radiocarbon dates from central North America. *Quaternary Research*, 72, 301–308.
- 1035 Guilloché, P., (1980). *Méthode de fabrication mécanique et en série des lames minces (2ème édit.)*.
1036 Paris, Grignon: CNRS et INA-PG.
- 1037 Hatté, C., Bréhéret, J.-G., Jacob, J., Argant, J., & Macaire, J.-J., (2013). Refining the Sarliève paleolake
1038 (France) neolithic chronology by combining several radiocarbon approaches. *Radiocarbon*, 55,
1039 979–992.
- 1040 Heiken, G., & Wohletz, K., (1985). *Volcanic ash*. Berkeley: University of California Press.
- 1041 Heiri, O., Lotter, A. F., & Lemcke, G., (2001). Loss on ignition as a method for estimating organic and
1042 carbonate content in sediments: reproducibility and comparability of results. *Journal of
1043 Paleolimnology*, 25, 101–110.
- 1044 Hirschberger, F., Fourmont, A., Macaire, J.-J., Bréhéret, J.-G., Guerin, R., & Bakyono, J.-P., (2006).
1045 Contribution of geophysical surveys to the study of fine grained lacustrine sediments .
1046 Application to the Sarliève marsh (Massif Central , France). *Bull. Soc. géol. France*, 177, 311–
1047 322.

- 1048 Joly, D., Brossard, T., Cardot, H., Cavailhes, J., Hilal, M., & Wavresky, P., (2010). Les types de climats
 1049 en France, une construction spatiale - Types of climates on continental France, a spatial
 1050 construction. *Cybergéo : European Journal of Geography*, 1–23.
- 1051 Jouannic, G., Walter-Simonnet, A. V., Bossuet, G., Cubizolle, H., Boivin, P., Devidal, J. L., & Oberlin, C.,
 1052 (2014). Occurrence of an unknown Atlantic eruption in the Chaîne des Puys volcanic field
 1053 (Massif Central, France). *Journal of Volcanology and Geothermal Research*, 283, 94–100.
- 1054 Juvigné, E., Bastin, B., & Gewalt, M., (1986). Découverte de retombées volcaniques d'âge Holocène
 1055 dans la Chaîne des Puys septentrionale (Massif Central, France). *Revue des Sciences Naturelles*
 1056 d'Auvergne, 52.
- 1057 Juvigné, E., & Gilot, E., (1986). Ages et zones de dispersion de téphra émises par les volcans du
 1058 Montcineyre et du Lac Pavin (Massif Central, France). *Zeitschrift deutschen geologischen*
 1059 *Gesellschaft* 137, 613–623.
- 1060 Kaufman, D., McKay, N., Routson, C., Erb, M., Dätwyler, C., Sommer, P. S., Heiri, O., & Davis, B.,
 1061 (2020). Holocene global mean surface temperature, a multi-method reconstruction approach.
 1062 *Scientific Data*, 7, 1–13.
- 1063 Kremer, K., Wirth, S. B., Reusch, A., Fäh, D., Bellwald, B., Anselmetti, F. S., ... & Strasser, M., (2017).
 1064 Lake-sediment based paleoseismology: Limitations and perspectives from the Swiss Alps.
 1065 *Quaternary Science Reviews*, 168, 1-18.
- 1066 Kylander, M. E., Ampel, L., Wohlfarth, B., & Veres, D., (2011). High-resolution X-ray fluorescence core
 1067 scanning analysis of Les Echets (France) sedimentary sequence: new insights from chemical
 1068 proxies. *Journal of Quaternary Science*, 26, 109–117.
- 1069 Kylander, M. E., Klaminder, J., Bindler, R., & Weiss, D. J., (2010). Natural lead isotope variations in the
 1070 atmosphere. *Earth and Planetary Science Letters*, 290, 44–53.
- 1071 Lavrieux, M., Disnar, J.-R., Chapron, E., Breheret, J.-G., Jacob, J., Miras, Y., Reyss, J.-L., Andrieu-Ponel,
 1072 V., & Arnaud, F., (2013). 6700 yr sedimentary record of climatic and anthropogenic signals in
 1073 Lake Aydat (French Massif Central). *The Holocene*, 23, 1317–1328.
- 1074 Lespez, L., Carozza, L., Berger, J., Kuzucuoğlu, C., Ghilardi, M., Carozza, J., & Vannière, B., (2016).
 1075 Rapid climatic change and social transformations Uncertainties, adaptability and resilience. In
 1076 *The Mediterranean Region under Climate Change-A Scientific Update* (p. 738). AllEnvi.
- 1077 Lindbo, D. L., Stolt, M. H., & Vepraskas, M. J., (2010). Redoximorphic Features. In *Interpretation of*
 1078 *Micromorphological Features of Soils and Regoliths* (pp. 129–147). Elsevier.
- 1079 Macaire, J. J., Fourmont, A., Argant, J., Bréhéret, J. G., Hirschberger, F., & Trément, F., (2010).
 1080 Quantitative analysis of climate versus human impact on sediment yield since the Lateglacial:
 1081 The Sarliève palaeolake catchment (France). *The Holocene*, 20, 497–516.
- 1082 Magny, M., (2004). Holocene climate variability as reflected by mid-European lake-level fluctuations
 1083 and its probable impact on prehistoric human settlements. *Quaternary International*, 113, 65–
 1084 79.
- 1085 Magny, M., Bossuet, G., Gauthier, É., Richard, H., Vannière, B., Billaud, Y., Marguet, A., & Mouthon,
 1086 J., (2007). Variations du climat pendant l'Âge du Bronze au centre-ouest de l'Europe : vers
 1087 l'établissement d'une chronologie à haute résolution. In C. Mordant, H. Richard, & M. Magny
 1088 (Eds.), *Environnements et cultures à l'Âge du Bronze en Europe Occidentale- Documents*
 1089 *préhistoriques n° 21* (p. 400). Besançon: CTHS.

- 1090 Martin, C., Ménot, G., Thouveny, N., Davtian, N., Andrieu-Ponel, V., Reille, M., & Bard, E., (2019).
 1091 Impact of human activities and vegetation changes on the tetraether sources in Lake St Front
 1092 (Massif Central, France). *Organic Geochemistry*, 135, 38-52.
- 1093 Martínez Cortizas, A., López-Merino, L., Bindler, R., Mighall, T., & Kylander, M. E., (2016). Early
 1094 atmospheric metal pollution provides evidence for Chalcolithic/Bronze Age mining and
 1095 metallurgy in Southwestern Europe. *Science of the Total Environment*, 545–546, 398–406.
- 1096 Mayoral, A., (2018). Analyse de sensibilité aux forçages anthropo-climatiques des paysages
 1097 protohistoriques et antiques du plateau volcanique de Corent (Auvergne) et de ses marges par
 1098 une approche géoarchéologique pluri-indicateurs. Université Clermont Auvergne.
- 1099 Mayoral, A., Berger, J. F., Peiry, J. L., Ledger, P., & Miras, Y., (2020a). Five millennia of human-
 1100 environment interactions reconstructed from pedosedimentary archives of the Lac du Puy
 1101 wetland (Corent, Fr.). *Catena*, 195, 104908.
- 1102 Mayoral, A., Granai, S., Develle, A. L., Peiry, J. L., Miras, Y., Couderc, F., Vernet, G., & Berger, J. F.,
 1103 (2020b). Early human impact on soils and hydro-sedimentary systems: Multi-proxy
 1104 geoarchaeological analyses from La Narse de la Sauvetat (France). *The Holocene*, 30, 1780–
 1105 1800.
- 1106 Mayoral, A., Peiry, J. L., Berger, J. F., Simon, F. X., Vautier, F., & Miras, Y., (2018). Origin and Holocene
 1107 geomorphological evolution of the landslide-dammed basin of la Narse de la Sauvetat (Massif
 1108 Central, France). *Geomorphology*, 320, 162–178.
- 1109 Miallier, D., Sanzelle, S., Pilleyre, T., Vernet, G., Brugière, S., & Danhara, T., (2004). Nouvelles données
 1110 sur le téphra de Sarliève et le téphra CF7, marqueurs chrono-stratigraphiques de Grande
 1111 Limagne (Massif central, France). *Comptes Rendus Geoscience*, 336, 1–8.
- 1112 Milcent, P.-Y., & Mennessier-Jouannet, C., (2007). Entre déterminisme environnemental et processus
 1113 historiques: formes et modalités d'occupation du sol en Basse Auvergne du Bronze Final au
 1114 début du second Age du Fer. In H. Richard, M. Magny, & C. Mordant (Eds.), *Environnements et*
 1115 *cultures à l'Âge du Bronze en Europe Occidentale- Documents préhistoriques n° 21* (p. 399).
 1116 Paris: CTHS.
- 1117 Miras, Y., (2016). HDR-Hétérogénéité des paysages de montagne, variabilités des systèmes
 1118 d'exploitation et transformations environnementales depuis le Néolithique : approches
 1119 intégratives, pluri-échelles et multi-proxies. Université Blaise Pascal.
- 1120 Monecke, K., Anselmetti, F. S., Becker, A., Schnellmann, M., Sturm, M., & Giardini, D., (2006).
 1121 Earthquake-induced deformation structures in lake deposits: A Late Pleistocene to Holocene
 1122 paleoseismic record for Central Switzerland. *Eclogae Geologicae Helvetiae*, 99(3), 343-362.
- 1123 Prat, B., (2006). Systèmes agropastoraux et milieux périurbains en Basse Auvergne au cours des trois
 1124 derniers millénaires: contribution de l'analyse palynologique à l'étude des interactions sociétés-
 1125 milieux. Thèse de doctorat, 368 pp.
- 1126 Raynal, J-P., Vernet, G., & Daugas, J., (2003). Evolution récente de la Limagne d'Auvergne (France) :
 1127 impacts du volcanisme et aspects des peuplements humains au Tardiglaciaire et à l'Holocène .
 1128 In C. Albore-Livadie & and F. Ortolani (Eds.), *Variazoni climatico-ambientali e impatto sull'uomo*
 1129 *nell'area circum-mediterranea durante l'Olocene, Territorio storico et ambiente 3* (pp. 461–
 1130 475). Bari: Edipuglia.
- 1131 Reimer, P. J., Austin, W. E. N., Bard, E., Bayliss, A., Blackwell, P. G., Bronk Ramsey, C., Butzin, M.,
 1132 Cheng, H., Edwards, R. L., Friedrich, M., Grootes, P. M., Guilderson, T. P., Hajdas, I., Heaton, T. J.,

- 1133 Hogg, A. G., Hughen, K. A., Kromer, B., Manning, S. W., Muscheler, R., Palmer, J. G., Pearson, C.,
 1134 Van Der Plicht, J., Reimer, R. W., Richards, D. A., Scott, E. M., Southon, J. R., Turney, C. S. M.,
 1135 Wacker, L., Adolphi, F., Büntgen, U., Capano, M., Fahrni, S. M., Fogtmann-Schulz, A., Friedrich,
 1136 R., Köhler, P., Kudsk, S., Miyake, F., Olsen, J., Reinig, F., Sakamoto, M., Sookdeo, A., & Talamo,
 1137 S., (2020). The IntCal20 Northern Hemisphere Radiocarbon Age Calibration Curve (0-55 cal kBP).
 1138 Radiocarbon, 62, 725–757.
- 1139 Riquier, V., Auxiette, G., Fechner, K., Loicq, S., & Toulemonde, F., (2015). Éléments de géographie
 1140 humaine et économique à l'âge du Bronze et au premier âge du Fer dans la plaine de Troyes.
 1141 Bulletin de la Société préhistorique française, 112, 339–367.
- 1142 Rodríguez-Pascua, M. A., Calvo, J. P., De Vicente, G., & Gómez-Gras, D., (2000). Soft-sediment
 1143 deformation structures interpreted as seismites in lacustrine sediments of the Prebetic Zone, SE
 1144 Spain, and their potential use as indicators of earthquake magnitudes during the Late Miocene.
 1145 Sedimentary Geology, 135(1-4), 117-135.
 1146
- 1147 Sabatier, P., Dezileau, L., Briquieu, L., Colin, C., & Siani, G., (2010). Clay minerals and geochemistry
 1148 record from northwest Mediterranean coastal lagoon sequence: Implications for paleostorm
 1149 reconstruction. Sedimentary Geology, 228, 205–217.
- 1150 Salminen, R., Batista, M. J., Bidovec, M., Demetriades, A., De Vivo, B., & De Vos, W., (2005). FOREGS
 1151 Geochemical Atlas of Europe, Part I* Background Information, Methodology, and Maps. Geol.
 1152 Surv. Finland, Espoo.
- 1153 Shanmugam, G., (2017). Global case studies of soft-sediment deformation structures (SSDS):
 1154 Definitions, classifications, advances, origins, and problems. Journal of Palaeogeography, 6,
 1155 251–320.
- 1156 Steig, E. J., (1999). Mid-Holocene climate change. Science, 286(5444), 1485-1487.
- 1157 Stockhecke, M., Sturm, M., Brunner, I., Schmincke, H. U., Sumita, M., Kipfer, R., ... & Anselmetti, F. S.,
 1158 (2014). Sedimentary evolution and environmental history of Lake Van (Turkey) over the past
 1159 600 000 years. Sedimentology, 61(6), 1830-1861.
- 1160 Stuiver, M., & Reimer, P. J., (1993). Extended 14C database and revised Calib 3.0 14C Age Calibration
 1161 program. Radiocarbon, 35, 215–230.
- 1162 Tinner, W., Lotter, A. F., Ammann, B., Conedera, M., Hubschmid, P., Van Leeuwen, J. F. N., & Wehrli,
 1163 M., (2003). Climatic change and contemporaneous land-use phases north and south of the Alps
 1164 2300 BC to 800 AD. Quaternary Science Reviews, 22, 1447–1460.
- 1165 Trément, F., Argant, J., Breheret, J.-G., Cabanis, M., Dousteyssier, B., Fourmont, A., Fournier, G.,
 1166 Liabeuf, R., Loison, G., Lopez-Saez, J.-A., Macaire, J.-J., Marinval, P., Mennessier-Jouannet, C.,
 1167 Milcent, P.-Y., Prat, B., Rialland, Y., & Vernet, G., (2007). Un ancien lac au pied de l'oppidum de
 1168 Gergovie (Puy-de-Dôme). Gallia, 64, 289–351.
- 1169 Trément, F., (2011). Les arvernes et leurs voisins du Massif Central à l'Époque Romaine-Une
 1170 archéologie du développement des territoires, vol. I. Clermont-Ferrand: Revue D'auvergne,
 1171 Alliance Universitaire d'Auvergne.
- 1172 Van Daele, M., Moernaut, J., Silversmit, G., Schmidt, S., Fontijn, K., Heirman, K., Vandoorne, W., De
 1173 Clercq, M., Van Acker, J., Wolff, C., Pino, M., Urrutia, R., Roberts, S. J., Vincze, L., & De Batist, M.,
 1174 (2014). The 600 yr eruptive history of Villarrica Volcano (Chile) revealed by annually laminated
 1175 lake sediments. Geological Society of America Bulletin, 126, 481–498.

- 1176 Vernet, G., (2005). Rapport final d'opération de diagnostic et de fouille archéologique, bassin de
1177 Sarliève, Grande Halle d'Auvergne (Cournon, Pérignat-les-Sarliève et Aubière). Centre
1178 archéologique de Clermont-Ferrand.
- 1179 Vernet, G., Henry, M. J., Cayrol, J., Parent, D., Wittmann, A., & Cabanis, M., (2011). COURNON, Puy-
1180 de-Dôme, Auvergne, Plaine de Sarliève. Rapport final d'opération de diagnostic. Centre
1181 Archéologique, Clermont-Ferrand.
- 1182 Vernet, G., (2013). La séquence sédimentaire des Gravanches / Gerzat : enregistrement
1183 d'événements «catastrophiques» à valeur chronologique en Limagne d'Auvergne (Massif
1184 Central, France). *Quaternaire*, 24, 109–127.
- 1185 Vernet, G., (2019). Les produits pyroclastiques distaux du volcan de la Nugère : synthèse des données
1186 et découverte en contexte archéologique. The distal pyroclastic products of the Nugère
1187 volcano : synthesis of data and discoveries in archaeological context. *Revue des Sciences
1188 Naturelles d'Auvergne*, 83, 3–34.
- 1189 Vernet, G., & Raynal, J.-P., (2002). Éruptions trachytiques de la Chaîne des Puys (France) et leur
1190 impact sur les environnements. In *Hommes et Volcans. De l'éruption à l'objet. XIVth Congress
1191 UISPP, Liege.*
- 1192 Wang, S., Ge, Q., Wang, F., Wen, X., & Huang, J., (2013). Abrupt climate changes of Holocene.
1193 *Chinese Geographical Science*, 23, 1–12.
- 1194 Witham, C. S., Oppenheimer, C., & Horwell, C. J., (2005). Volcanic ash-leachates: A review and
1195 recommendations for sampling methods. *Journal of Volcanology and Geothermal Research*,
1196 141, 299–326.
- 1197 Yansa, C., & Long, D., (2007). Improving the Accuracy of Radiocarbon Chronologies from Lake-
1198 sediment Cores: Testing for the 14C Reservoir Effect in Aquatic Macrophytes-CWS Venture
1199 Grant- Report of Findings.
- 1200 Zielhofer, C., Köhler, A., Mischke, S., Benkaddour, A., Mikdad, A., & Fletcher, W. J., (2019). Western
1201 Mediterranean hydro-climatic consequences of Holocene ice-rafted debris (Bond) events.
1202 *Climate of the Past*, 15, 463–475.
- 1203
- 1204
- 1205